

Some Comments on the Analysis of “Big” Scientific Time Series

This paper examines climate, geomagnetic, interplanetary, and seismic data closely and summarizes the resulting conclusions.

By DAVID J. THOMSON, *Life Fellow IEEE*, AND FRANK L. VERNON, III

ABSTRACT | Experience with long time series from space, climate, seismology, and engineering has demonstrated the need for even longer data series with better precision, timing, and larger instrument arrays. We find that almost all the data we have examined, including atmospheric, seismic data, and dropped calls in cellular phone networks contain evidence for solar mode oscillations that couple into Earth systems through magnetic fields, and that these are often the strongest signals present. We show two examples suggesting that robustness has been overused and that many of the extremes in geomagnetic and space physics data may be the result of a superposition of numerous modes. We also present initial evidence that the evolution of turbulence in interplanetary space may be controlled by modes. Returning to the theme of “big data,” our experience has been that theoretical predictions that spectra would be asymptotically unbiased have turned out to be largely irrelevant with very long time series primarily showing that we simply did not understand the problems. Data that were considered to have excessively variable spectra appear to evolve into processes with dense sets of modes. In short data blocks, these modes are not resolved and as the relative phase of the modes within the estimator varies, so does the apparent power. Ideas that data series become uncorrelated at modest distances in either

time or space do not seem to be true with the long duration continuous time series data we have examined.

KEYWORDS | Data processing; seismology; spectral analysis; statistical analysis; Sun; time series analysis

I. INTRODUCTION

This paper is concerned with changes in the analysis of scientific time series data implicit in “big data” with examples from seismology, climate, space physics, and engineering.

Our experience is that, in these fields, the requirement for precision instruments has, if anything, increased. In addition to the number of samples that can be acquired in a scalar time series, the precision of the data and the dimensionality have increased as well. In the early 1970s, a continuous series of a million samples was rare, but are now routine and getting on the small side.

All of these influence how one analyzes data. In our experience, much of the analysis occurs in the frequency domain where increases in precision and sample size put increasing demands on spectral analysis and related methods. The hope that large enough samples would cause relatively simple estimates of spectral densities to converge to something useful, i.e., [1]–[4], has been overwhelmed by the increasing complexities revealed by the improved and larger data. John W. Tukey once remarked (approximately) “Don’t spend too much time on asymptotics because the only reason that anyone will go to the trouble and expense of collecting large amounts of data is because they are going to ask harder questions.”

Manuscript received December 2, 2015; accepted March 2, 2016. Date of publication September 28, 2016; date of current version October 18, 2016. The work of D. J. Thomson was supported by the Natural Sciences and Engineering Research Council of Canada (NSERC), by the Canada Research Chairs Program, by the Canadian Statistical Sciences Institute (CANSSI), and by the Bonneville Power Administration under Grant TIP-290. This material is based upon work supported by the Incorporated Research Institutions for Seismology under their Cooperative Agreement EAR-0733069 with the National Science Foundation.

D. J. Thomson is with the Department of Mathematics and Statistics, Queen’s University, Kingston, ON K7L 3N6, Canada (e-mail: djt@mast.queensu.ca).

F. L. Vernon, III is with IGPP, Scripps Institution of Oceanography, University of California at San Diego, La Jolla, CA 92093 USA (e-mail: flvernon@ucsd.edu).

Digital Object Identifier: 10.1109/JPROC.2016.2598218

0018-9219 © 2016 IEEE. Personal use is permitted, but republication/redistribution requires IEEE permission. See http://www.ieee.org/publications_standards/publications/rights/index.html for more information.

The largest single change that we have observed with “big data” is in our approach to *science*. Traditionally, one often had a specific hypothesis or question in mind, e.g., “can we detect a particular mode in this data?” followed by “what is its frequency and Q?” An early foray into “big data” time series [5], [6] was given by the development of the WT4 millimeter waveguide system [7] at Bell Labs. The dominant loss mechanism in this waveguide was from mode conversion, with the loss proportional to the power spectrum of the distortion. There were many propagating modes, and the various spectra were estimated from *mechanical* measurements [8] of the geometry of individual sections of waveguide. A combination of manufacturing, shipping, and field considerations limited the length of individual waveguides to about 9 m so a dominant concern at the time was how to obtain accurate estimates of spectra from such short samples. There were between 1 and 30 series of mechanical measurements on individual waveguide, each between 900 and 5000 samples, and more than 1500 different waveguides. The goal was initially simple: “does this piece of waveguide meet our quality specifications?” with the major specifications bounded by limits on the spectrum of geometric distortions. Attempts to discover why individual sections failed quickly converted this simple goal into more complex estimates. One notes, incidentally, that the first goal involved sampling distributions and these were built into the specifications but, once these were violated and one entered the “detective” phase, exact statistical distributions were almost irrelevant. Finally, at the field-trial stage [9], the individual sections were welded together to give a 14-km test run. This was measured mechanically at a 1-cm rate to produce series of horizontal and vertical curvature and diameter, each approximately 1.4 million samples, “big” by the standards of the 1970s.

Currently, the question is more “what exotic features are suggested by this data and do we have analysis tools to describe them?” One should remember that modern spectrum estimates, as described in most texts, are conceptually identical to what was suggested by Sir G. G. Stokes in 1878 [10]. Although numerous extensions to the basic theory have been proposed, such as: coherence [11]; bispectra [12] and the families of “higher order” spectra [13], and improvements in estimators, analysis of nonstationary series is still more art than science. With such data, more apropos estimates are often obtained by iterating the basic spectrum estimation procedure. That is, one computes a series of spectrum estimates, extracts some parameters of interest from each, then treats these as a new time series. This can usually only be done in big data situations. Some of these new tricks are described in Section X-B and C.

This paper provides a brief review of the theoretical background for multitaper spectral analysis, coherence, and similar functions followed by examples of involving

large amounts of data. “Large” can be used here to describe two distinct phenomena: first, the obvious one where there are so many observations that they become computationally or graphically cumbersome; second, the more interesting cases where the number of observations is modest, but have a relatively long duration and are often the longest such data set known. Examples include the Burgundian Pinot Noir grape harvest dates [14] (Section VIII-B) and the Uppsala daily temperature record (Section X-E).

II. WHAT IS “NOISE”?

A major goal of both acquiring and analyzing data is to improve the “signal-to-noise” ratio. If you are fortunate enough to have a description of the noise in your data that starts with kT , where k is Boltzmann’s constant and T is the temperature in Kelvins and analysis shows residuals within a decibel or two of this level, you can skip the rest of this section. Most of us, however, are not so fortunate and characterizing “noise” is a major task. We give two specific examples.

- 1) In seismic data, “noise” on the two horizontal components is often 10 dB (or more) higher than it is on the vertical [15] although all three components may be derived from identical sensors. A possible explanation was given in [16].
- 2) In magnetotellurics and the related problem of estimating induced voltages and currents on power lines and pipelines from changes in the geomagnetic field, *improper* complex-valued data effectively generates a “noise” field with a similar magnitude as the proper data [17].

Based on these and similar observations, a major change in our outlook is that much of what used to be considered “noise” in many different kinds of data appears to originate in normal modes of the Sun. Solar modes are systematic oscillations of the Sun’s interior excited by turbulence in the convection zone and which resonate at frequencies from $\sim 0 \mu\text{Hz}$ to $\gtrsim 5000 \mu\text{Hz}$. These were first noticed in the process of investigating a series of communications satellite anomalies during the active solar maximum around 1990. This was followed by a study of data from the *Ulysses* spacecraft augmented with some from *Voyager II* and other spacecraft, where it was found that much of the variability in the solar wind occurred at discrete frequencies. The higher frequencies, those with periods near 5 min, agreed closely with those of optically measured p -modes, while at lower frequencies they were similar to those predicted for gravity, or g -modes [18]. Given the prevailing dogma that the solar wind was turbulent, this paper was considered to be heresy and was attacked. Additional evidence countering these attacks was given in [19], and simulations described in [20] showed that discrete modes and turbulence could coexist. Compounding the heresy,

Thomson [21] suggested that the strongest *observational* evidence for turbulence in the solar wind, the $-5/3$ spectral index¹ of many power spectra in the solar wind was a misattribution. What was being observed was a fossil of turbulence in the solar convection zone.

During the time that the events of the preceding paragraph were occurring in the space physics and engineering literature, three papers [22]–[24] appeared in the seismic literature showing that the Earth’s normal modes were continuously excited. More importantly, all three of these discovery papers noted the presence of unusual modes in their data. These papers on “seismic hum” launched a small industry attempting to find a mechanism that provided sufficient energy, roughly that of a magnitude 6 earthquake *every day*, to excite the modes. Inexplicably, particularly in view of the fact that normal modes of the Earth have been studied since Lord Kelvin’s 1863 dispute with geologists on whether Earth’s interior was primarily solid [25] or liquid [26] (see the history of this endeavour and the subsequent development of normal mode theory in [27, Ch. 1]), the observations of the unexplained modes were largely ignored. Normal mode seismology is a mature theory with many modes having been predicted and most of the predicted ones observed (see, e.g., [28] and [29] for a recent update), so the discovery of new modes should have been taken far more seriously than it was.

We began studying this phenomenon in 2001, attributing the strange modes to solar forcing at the AGU fall meeting in 2007 [30], [31] and, after numerous delays, published [16], [32]. The majority of these delays resulted from surprises in the data; it seemed that every time one looked at a new kind of data (or pairings of data sets) there was something new to explain. Was it a fluke, could we explain it, was it repeatable in other data sets, was there anything in the literature, and so on? Other delays were incurred by having to rewrite code that scaled poorly from a few hundred hours of data to years of data. An additional factor was the problem that these long data sets started to resolve the discrete solar modes in unexpected places. Their presence definitely complicates matters because Harvey [33] estimates that there are ten million solar modes, so even if only the low-degree modes are reasonably resolved one must still consider many modes and one suspects that much of the “noise” between larger peaks may be mostly due to unresolved higher degree modes. In such spectra, “smoothing” the estimate in the manner that has been common since the 1940s made an already complicated problem worse. The basic problem is that the “raw” multitaper estimates of spectra or coherence were high at modes, low between modes, and smoothing produced an estimate that was “wrong

everywhere.” Nonetheless, Thomson and Vernon [16] show clear evidence that “Earth’s hum comes from the Sun,” with coupling, most probably, through the interplanetary magnetic field. However, because the solar wind density, velocity, composition, and temperature all show strong modal features these components are almost certainly involved as well. This coupling both explains the unexpected modes noted in the three hum discovery papers (they are normal modes of the Sun) and also implies that there is more than sufficient energy to drive the observed hum. In addition to the numerous examples given in [34], work in progress shows evidence for solar modes in barometric pressure [35], [36], ground-level ozone, and numerous other kinds of data. Daily data are not exempt because aliases of *g*-modes are readily detectable in solar noon 10.7-cm flux, [37]. Other low frequency solar modes can be measured both in interplanetary data [18] and daily temperatures [38], [39].

Taken together, the preceding paragraphs summarize the beginnings of a revolution in our understanding of “noise.” Before this, it was common to assume that quantities such as barometric pressure, surface air temperature, ground-level ozone concentration, or seismic noise would be uncorrelated for measurements separated by modest distances in either time or space. Most statistical models of time series use low-order autoregressive or moving average models (or their offshoots), all with reasonably fast mixing properties. From our viewpoint, however, one expects (and sees) correlations across continental and interplanetary scales. The departures from predictions from fast mixing in the time domain are even more extreme: at periods of a few minutes one expects to see solar *p*-modes. These modes are randomly excited and, depending on the mode, having damping times of a few days to months. At lower frequencies, those corresponding to periods from several days down to ~ 30 min, one finds evidence for solar gravity modes. These are predicted [40] to have damping times between 10^5 and 10^7 years. Thus, instead of stationary mixing noise, one has a dense thicket of high-*Q* modes as a background in many applications. Very few of these modes have been identified [41], in the sense of assigning “quantum numbers” to them, so one is often faced with a bewildering forest of peaks in a spectrum. The frequencies of solar *p*-modes were found to vary with solar activity in [42] and the frequencies, line widths, etc., studied in numerous papers, e.g., [43]–[48]. The Sun’s acoustic cutoff frequency also varies by ~ 100 to ~ 150 μHz with activity [49] so the number of *p*-modes that are observed will also vary with activity. Similarly, the frequencies of *g*-modes are also predicted [50] to vary with irradiance. Consequently, taking exceptionally long series will give the expected improvement in frequency resolution, but this may not correspond to an improvement in detectability because the mode’s frequency may shift out of the resolution bandwidth. To conclude this section, we note

¹The spectral index is the slope of a spectrum on a log-power versus log-frequency plot. An index of $5/3$, corresponding to a spectrum with the shape $c/f^{5/3}$ over a wide frequency range, is commonly taken as the “signature” of Kolmogorov turbulence.

that although solar modes can have exceptionally long lifetimes, they are described using essentially Newtonian mechanics and have nothing to do with “long-memory” processes [51], [52].

III. STATIONARITY

The rise of big data is changing our understanding of stationarity. The increasing availability of continuous time series creates opportunities for nonstationary processes to be observed and identified. Going forward, stationarity will play much the same role as Gaussian distributions. It is useful because stationarity, particularly when combined with the Gaussian assumption, allows one to do analysis where the resulting formulas are simple enough to understand. The importance of having such results is difficult to underestimate, but they must always be used in combination with Martin Wilk’s comment “The hallmark of good science is that it uses models and theories but never believes them.”

IV. SOME HISTORY

Looking back over the past few decades, a major change has occurred from simply trying to estimate a spectrum, to concentrating on descriptive statistics of the spectrum estimates. As a specific example, in the discussion of [53] Dr. I. T. Jolliffe commented on “the large number of peaks that appear in the spectral estimates.” However, we had gone out of our way to choose relatively simple examples, ones with no more than half a dozen or so peaks. The data series used in those examples were all relatively short, 1000 samples or less. In much recent data, data blocks of 50000–500000 samples are routine and we would be surprised if the spectrum contained less than a few hundred significant peaks and finding several thousand lines is not unusual. This implies many changes.

First, [53] was published in 1979, before the invention of the multitaper estimate in [54] in 1982, so the spectrum estimates being considered were single-taper direct estimates. Spectrum estimates made with a single data taper have a nominal χ_2^2 distribution, that is chi-squared with two degrees of freedom (DoF), and so have atrocious sampling properties such as large variance. If one has a sample of M χ_2^2 independent random variates z_i , all with mean 1, their minimum is expected to be $E\{z_{\min}\} = 1/M$ while their maximum $E\{z_{\max}\} \sim \ln M + \gamma + (1/2M)$ where $\gamma = 0.57721566\dots$ is Euler’s constant. In other words, one expects the ratio of largest to smallest values in a random sample to be $\sim M \ln 1.78M$ so, for $M = 100\,000$, the range of the spectrum estimates will be 1.2×10^6 . We emphasize that this is in white noise with absolutely nothing interesting happening.

Second, if one is doing exploratory spectrum estimation and takes, for example, the 99% significance level

as an initial threshold for “interesting” features one knows by definition that about 1% of the estimates will lie above it. Single-taper estimates, however, tend to distribute this 1% in two narrow peaks per Rayleigh resolution [36, Fig. 2], so our hypothetical spectrum will have ≈ 2200 spurious peaks above the 99% level.

Third, it was proven by Rayleigh [55] that the periodogram is inconsistent, that is, its variance does not decrease with sample size. This applies to all single-taper spectrum estimates.

Fourth, the sidelobes of many direct estimates [56] are so high that these estimates cannot cope with the range of much modern data. For example, the spectrum of the barometer data shown in [36, Fig. 1] has a range $\gtrsim 10^{13}$ so many estimates will be biased by several orders of magnitude. The variance of a direct estimate is roughly the square of its expected value $(EV + \text{bias})^2$, so it may be too high by ridiculously large factors. These are not the sampling statistics one needs for scientific discovery or engineering analysis. In contrast, the sampling properties of a multitaper estimate with 20 DoF have a lower, 0.001%, point of 0.166 and an upper, 99.999%, point of 2.952. For the $M = 100\,000$ sample example considered above, this reduces the range from $> 10^6$ to ~ 17.8 and the ≈ 2200 spurious peaks above the 99% level to about 730.

During approximately the same time interval, there was a similar improvement in instrumentation. As a specific example, the spectral windows plotted in Blackman and Tukey’s 1958 book on spectrum estimation, covered such a small range that many have been plotted on a *linear* scale where one can see the sidelobes; see, e.g., [57, Figs. 15(f) and 21(a)]. Similarly, the appendix of Bogert *et al.*’s 1967 paper introducing the cepstrum [58] contains a comparison of hand and digital voltmeter digitization of seismic records to three decimals. Progress, however, was rapid and, e.g., the gauging system for WT4 millimeter waveguide [8] was routinely producing 25-b data by 1975. The analysis of this high-quality data drove developments in robustness, required the efficient prolate data tapers [5], [6], and led to the development of multitaper methods [54].

While the impetus for the development of multitaper spectral analysis techniques was driven by the WT4 millimeter waveguide analysis, many other instrumentation, computing, and communications innovations started driving the need for these tools to analyze big data. In the context of this paper, we extend the use of the term “big data” beyond a large number of bytes to include long time series spanning years of continuous data, high dynamic range data, data arrays created by thousands of sensors, and the integration of multidisciplinary sensor types.

Since this paper is focused on “big data” applications of multitaper spectral analysis, it is important to start in the time domain where the original data are recorded. To maximize the efficiency of any spectral technique, it is necessary to maintain a constant sampling rate. For finite duration local experiments, this has been a tractable

problem for many years. However, when we shift to long-term continuous measurements on a global scale, this becomes a very difficult problem. Radio time-synchronization services started in the 1960s with the introduction of time information into WWV, WWVB [59] and their international siblings introduced the possibility of distributed timing accuracies of 1 ms for WWV and 0.1 ms for WWVB. The advent of GPS-based time synchronization systems improved time accuracy for distributed systems to better than 1 μ s [60]. Due to size and power requirements, long-term continuous measurement and observing systems needing accurate timing also had an implicit requirement for continuous line power, preferably with some form of uninterruptible power supply. In the late 1990s, low-power GPS-based clocks started to become available that allowed for continuously disciplined clock oscillators, eliminating the need for timing corrections in systems that used them. Coupled with the rapid evolution of low-power integrated circuits, we see an escalation of distributed sensor networks with high-quality time resolution.

One important attribute of multitaper spectral analysis is the capability to investigate data with high dynamic range. Commercially available analog-to-digital converters (adc) based on integrated circuits, digital data acquisition systems using 8-b adc with 48-db dynamic range started to be available in the 1970s and have evolved to the now ubiquitous 24-b adc with 144-db dynamic range. In parallel, passive electromechanical sensors have transitioned into high-dynamic range active feedback sensors matching the increased dynamic range provided by each generation of adc.

Other factors needed to generate large data sets to be processed by multitaper-driven algorithms include improved computation, storage, and communications. Computationally, processors transitioned from typically 16-b platforms in the 1970s to the current standard 64-b platforms that are now able to easily handle the computational requirements. Local low-power flash storage at remote field sites is now on the order of terabytes and at data centers large numbers of terabyte to petabytes of data storage are now available. For distributed sensor networks there are now IP networks over wireless and satellite communications that provide for essentially lossless data telemetry if an appropriate retransmission protocol is used. In the wired environment, the use of fiber optics can enable effective use of cloud computing and cloud storage for large scale computing problems.

The confluence of high quality time and the ability to record long gap-free time series with high dynamic range systems, coupled with advances in computing, storage, telemetry, communication, and power systems create the opportunity to effectively use multitaper spectral analysis techniques on large data sets. One example system is the NSF Earthscope USArray Transportable Array (TA). This system was designed to simultaneously record 400

autonomous stations with real-time telemetry in continuous time series. In total, 1738 TA stations were deployed in a nominal 70-km grid starting in the western United States in 2004 and rolling eastward across the contiguous 48 states finishing in 2015 (Fig. 1). The TA in the continental United States had a median station deployment time of one year and 315 days. The longest operational station is still currently operating for 11 years and 207 days. All stations were sampled with GPS continuously disciplined clock oscillators providing better than 1- μ s timing accuracy across the whole sensor network. As of the time of this writing, in total 1 290 101 station days of continuous data have been recorded, with 26 206 unique science sensor station channels and 36 639 unique system state-of-health channels. To date, over 17.7 terasamples of science data has been recorded using 70.8 TB of storage (23 TB using lossless compression). To date, these TA data have been used in over 100 Ph.D. dissertations and 200 refereed journal papers, so we will not even attempt to summarize it here.

Currently, in looking for “descriptive” summaries of power spectra it is becoming common to iterate the process. The first example of such a procedure that we know, the cepstrum [58], took a Fourier transform of the logarithm of an estimated spectrum to find an echo. This was rapidly generalized [61], and today one might use a second multitaper estimate and *F*-test to identify an echo. Second, taking the SVD of a log-spectrogram [62] decomposes the matrix into left and right eigenvectors where, e.g., the left eigenvectors are simply new time series. Computing their spectra often shows systematic features in nonstationary data. In Section X-B, we show a more direct approach with spectral indices of interplanetary data.

V. INITIAL DATA SCREENING

Almost the first advice given in any text on time series analysis or multivariate statistics is “plot the data.” We agree with this but, with large amounts of data, there are practical difficulties: First, both graphical devices and the human eye have finite resolution, so plotting a million-sample time series on a device with a resolution of a few thousand pixels is pointless. Second, the point of plotting the data is to spot outliers, instrument malfunctions, data gaps, and regions that appear different from the rest and, possibly excluding large outliers, this cannot be done without adequate graphical resolution. Third, this advice is given for a good reason: the number of things that can go wrong is so large that it does not seem possible to categorize them or to automate detection. The human eye and brain seems to be the best general pattern recognition device available, so plot the data. Fourth, this too has limitations; plotting data at high enough resolution to see peculiar features often requires the equivalent of several hundred plots, and looking through such a mass of data produces fatigue, so

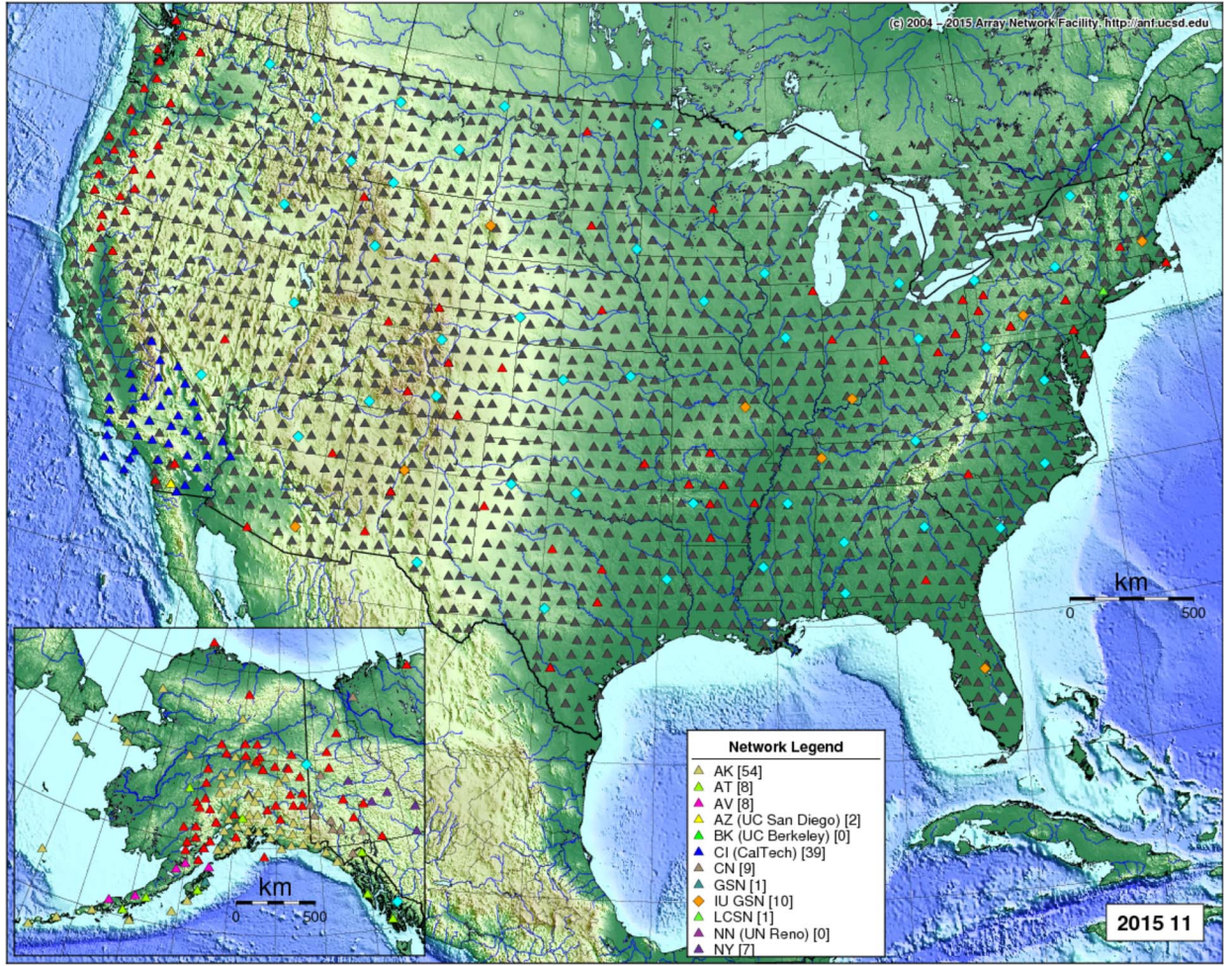


Fig. 1. Cumulative deployment of USArray Transportable Array from 2004–2015. Core TA stations are shown as red triangles (operating) or gray triangles (decommissioned). Other contributed stations from other networks are identified in the Network Legend box.

anomalies on the first frame or two will probably be detected, those on the equivalent of frame 450 may not be.

This has resulted in a variety of methods for screening data ranging from simple plots of order statistics, to running Karhunen–Loève expansions, multitaper spectrograms, and coherences, which are appropriate for big data problems.

VI. TECHNICAL BACKGROUND

To make the following sections comprehensible we need some notation so we begin with a short section on random processes and one on Slepian sequences. Assume one is given a sample of data $x(t)$ for $t = 0, 1, \dots, N - 1$ from some physical process for the purpose of estimating a spectrum. The spectrum is a function of frequency, denoted by f that, for a unit sampling rate $\delta t = 1$, has principal domain $[-(1/2), (1/2))$. Note that f is ordinary cyclic frequency, not radian frequency. That is, if $\delta t = 1$ s, then f is in units of cycles per second, defined in the S.I. system as Hertz (Hz). Note that frequency is usually

considered to be real valued, but can be complex valued. We now take the Fourier transform of the time series

$$y(f) = \sum_{t=0}^{N-1} x(t) e^{-i2\pi ft}. \quad (1)$$

The Fourier transform is a trivially sufficient statistic because one may take the inverse Fourier transform

$$\int_{-\frac{1}{2}}^{\frac{1}{2}} y(f) e^{i2\pi ft} df = \begin{cases} x(n), & 0 \leq n \leq N - 1 \\ 0, & \text{otherwise} \end{cases} \quad (2)$$

and recover the data.

We now assume that the sample is from a second-order (or covariance) stationary random process. In this section,

we also assume (see Section VIII-A) that the process is zero mean, that is $\mathbf{E}\{x(t)\} = 0$: this implies that $\mathbf{E}\{dX(f)\} = 0$, where $\mathbf{E}\{\cdot\}$ denotes the expected value operator. This further implies a spectral representation [63]–[65]

$$x(t) = \int_{-\frac{1}{2}}^{\frac{1}{2}} e^{i2\pi\xi t} dX(\xi) \quad (3)$$

for the process. The spectrum is a decomposition of variance into a function of frequency, i.e., the average power in a small band $(f, f + df)$, and is formally defined [64] in terms of the spectral representation as

$$S(f)df = \mathbf{E}\{|dX(f)|^2\}. \quad (4)$$

The stationarity assumption implies that the autocovariance function

$$R(\tau) = \mathbf{E}\{x(t + \tau) \cdot x^*(t)\} \quad (5)$$

is not a function of time t , and this has the further implication that

$$\mathbf{E}\{dX(f) dX^*(\xi)\} = S(f) \delta(f - \xi) df d\xi \quad (6)$$

where $\delta(\cdot)$ is the Dirac delta function. Stationarity requires that signal elements at distinct frequencies be uncorrelated. One also notes that, using the spectral representation (3) in (5), then applying (6), gives

$$R(\tau) = \int_{-\frac{1}{2}}^{\frac{1}{2}} S(f) e^{i2\pi f\tau} df \quad (7)$$

the Einstein–Wiener–Khinchine theorem. (It was discovered independently by Wiener [11] and Khinchine [66] in the 1930, but Einstein [67] had preceded them in a short note in 1914. The great Russian probabilist Yaglom [68] commented that Einstein’s derivation is more satisfactory than either of the former two.)

When the process is nonstationary but harmonizable, (6) must be replaced with the Loève spectrum and one has

$$\mathbf{E}\{dX(f_1) dX^*(f_2)\} = S_L(f_1, f_2) df_1 df_2. \quad (8)$$

This was introduced by Loève in the 1940s (see the references in [69]) but, recalling that stationary processes were still considered difficult and obscure, they have not been used as much as they should have been. Rotating the (f_1, f_2) coordinates by 45° and taking a Fourier transform on the “nonstationary” frequency gives a spectrogram.

One must be cautious in using spectral representations for reasons originally noted in [70], and commented on in [13]. Also remember that the spectral representation is accurately named; it is a *representation* whose main use is as a mathematical tool for assessing properties of estimators. We would be surprised to learn of a physical process that originates in such a way.

A. Slepian Sequences

In a famous set of papers entitled *Prolate Spheroidal Wave Functions, Fourier Analysis, and Uncertainty* begun in 1965 [71], Slepian, Landau, and Pollak established bounds on simultaneous time-frequency concentrations, the uncertainty principle when boundaries are imposed. Part five (V) of this series [72] described the discrete case where one has N time points at $t = 0, 1, \dots, N - 1$ and continuous frequency $-(1/2) \leq f < (1/2)$. Given a unit norm sequence v_t , defined on $[0, N - 1]$, the integral of its magnitude-squared Fourier transform $V(f)$ over the Nyquist band $[-(1/2), (1/2))$ is, by Parseval’s theorem, also unity, that is

$$1 = \sum_{t=0}^{N-1} |v_t|^2 = \int_{-\frac{1}{2}}^{\frac{1}{2}} |V(f)|^2 df. \quad (9)$$

Slepian found the sequences with the largest fraction of their energy λ_k , in the frequency band $(-W, W)$, that is

$$\lambda = \int_{-W}^W |V(f)|^2 df \quad (10)$$

and the optimum sequences are the discrete prolate spheroidal sequences (DPSSs), now known as Slepian sequences. They are the real, orthonormal eigenvectors of the Toeplitz matrix eigenvalue equation

$$\lambda_k(N, W) v_t^{(k)}(N, W) = \sum_{n=0}^{N-1} \frac{\sin 2\pi W(t - n)}{\pi(t - n)} v_n^{(k)}(N, W). \quad (11)$$

They are ordered by their corresponding eigenvalues $1 > \lambda_0 > \lambda_1 > \dots > \lambda_{N-1} > 0$, with λ_k giving the energy

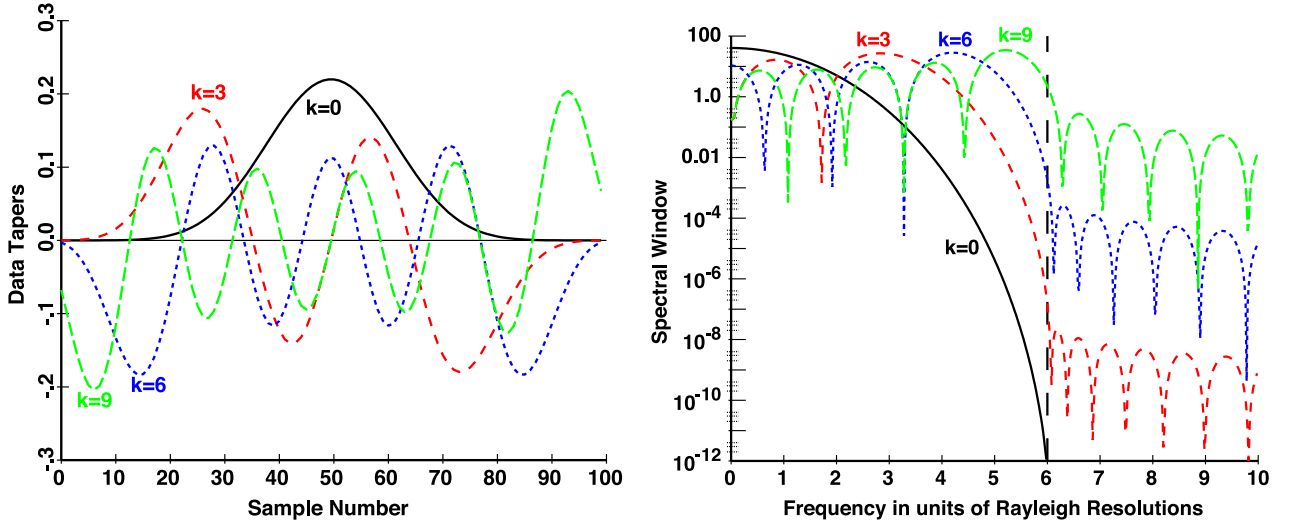


Fig. 2. The left panel shows Slepian sequences for $NW = 6$, $N = 100$, and $k = 0, 3, 6$, and 9 . The right panel has the corresponding spectral windows $|V_k(f)|^2$ with frequency expressed in units of Rayleigh resolutions, and the dashed vertical line showing the positive bandedge. The total power in the outer band for the k th sequence is $1 - \lambda_k$, here 2.9×10^{-14} , 4.7×10^{-10} , 6.7×10^{-6} , and 0.011 for the sequences shown. The zeroes of the $k = 3$ and $k = 9$ functions at the origins are suppressed and the sidelobe levels are clipped below 10^{12} .

concentration of the k th sequence in $(-W, W)$. Also, the k th sequence has k zero crossings in $[0, N - 1]$ and the corresponding Slepian functions

$$V_k(N, W; f) = \sum_{n=0}^{N-1} v_n^{(k)}(N, W) e^{-i2\pi n f} \quad (12)$$

have k zeroes in $(-W, W)$; see Fig. 2. The functions are doubly orthogonal, first on the full frequency range

$$\int_{-\frac{1}{2}}^{\frac{1}{2}} V_j(N, W; f) V_k^*(N, W; f) df = \delta_{j,k} \quad (13)$$

and, second, on the inner (or local) band

$$\int_{-W}^W V_j(N, W; f) V_k^*(N, W; f) df = \lambda_k \delta_{j,k}. \quad (14)$$

That is, they are orthonormal on $[-(1/2), (1/2))$, and orthogonal on $(-W, W)$. We omit the explicit dependence on N and W so, e.g., the k th sequence is denoted by $v_t^{(k)}$ and the eigenvalues by λ_k . Of these, the first $K \approx \lfloor 2NW \rfloor$ eigenvalues are extremely close to one and, for example, with $NW = 6$, $1 - \lambda_0 \approx 1.31 \times 10^{-15}$ and with $NW = 10$,

$1 - \lambda_0 \approx 3.05 \times 10^{-26}$. Section VI of [34] and Fig. 3 in this paper show estimates of spectra of barometer data where the range (max/min) is $\sim 10^{16}$, with the bulk of the power at very low frequencies, so ordinary spectrum estimates are dominated by bias from the low frequency range. In this case, tapers with extremely strong out-of-band suppression are needed, and the Slepian sequences serve nicely.

Slepian's analysis defines the dimensionality of the time-frequency region $[0, N - 1] \times (-W, W)$. Many of the properties of Slepian sequences depend on the time-bandwidth product $C_R = NW$ as opposed to N and W individually. The $K = 2NW = 2C_R$ lowest order sequences are a complete bases for this subspace. In spectrum estimation problems, W is the bandwidth of the estimate and is a factor of C_R , typically 2 to 10, of the Rayleigh resolution,² $\mathcal{R} = 1/(N\Delta t)$. As N increases, properties of the Slepian sequences rapidly approach those of the continuous-time prolate spheroidal wave functions. Details are given in [72], and Appendix A of [73] gives a summary. Finally, note that while (11) is analytically convenient, it is not recommended for numerical use. To compute the sequences we use the tridiagonal form with separate calculations of the odd and even sequences given in [73, App. B].

The choice of C_R determines the number of tapers $K \sim \lfloor 2C_R \rfloor$, the degrees of freedom $\nu \approx 2K \lesssim 4C_R$, and bias properties of the estimate. The broadband bias, i.e.,

² C_R seems to be increasing in time. In [54], $C_R = 4$ was “standard” but the spectral range of modern data often requires $C_R \geq 8$ or 10, even with prewhitening.

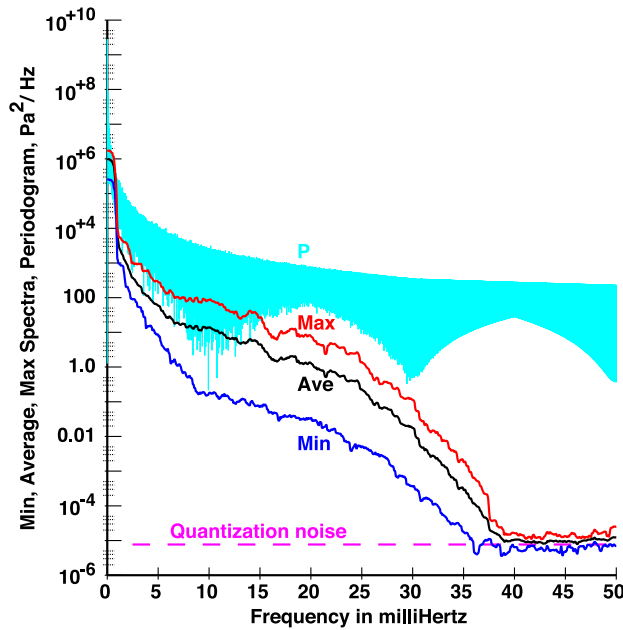


Fig. 3. Spectrum estimates for eight adjacent sections of 1000 samples each of barometric pressure data from the Black Forest Observatory. The top “curve” (cyan) is the periodogram from the first section. The three lower curves are the minimum, arithmetic average, and the maximum of the eight multitaper estimates. These were computed with $NW = 10$ and $K = 12$ tapers on each section. Note that above 35 mHz the periodogram is biased by a factor of $> 10^7$. Any estimate based on sample autocovariances will have similar bias problems as the periodogram.

the bias at f contributed by frequencies outside the band $(f - W, f + W)$, decreases exponentially with C_R .

VII. MULTITAPER SPECTRUM ESTIMATES

Temporarily shifting the origin of the Fourier transforms in (3) and (1) to the center of the observation interval, that is, $\bar{t} = (N - 1)/2$, so replacing t with $t - ((N - 1)/2)$ in these two equations and merging them gives

$$y(f) = \int_{-\frac{1}{2}}^{\frac{1}{2}} \frac{\sin N\pi(f - \xi)}{\sin \pi(f - \xi)} dX(\xi) \quad (15)$$

so the Fourier transform of the data can be written in terms of the spectral representation, giving what Parzen has called “the fundamental equation of spectrum estimation.” It is a convolution of the Dirichlet (or diffraction) kernel and dX .

In multitaper analysis one thinks of (15) as an integral equation and attempts to solve it. Recognizing that a unique solution is impossible, one goes for the best one

can get. This is done by local least squares in a band $(f - W, f + W)$, with sequential bands estimated by sliding the band along in frequency. Recalling the standard method of solving Fredholm integral equations of the first kind, the eigencoefficients (the coefficients of the eigenfunctions) are defined by

$$y_k(f) = \frac{1}{\lambda_k} \int_{-W}^W y(f - \xi) V_k(\xi) d\xi. \quad (16)$$

After some algebra this becomes

$$y_k(f) = \sum_{t=0}^{N-1} x(t) v_t^{(k)} e^{-i2\pi ft} \quad (17)$$

the standard definition of the eigencoefficients. The k th eigencoefficient is thus the Fourier transform of the data multiplied by the k th Slepian sequence. We denote its squared magnitude by

$$S_k(f) = |y_k(f)|^2 \quad (18)$$

the k th eigenspectrum.

In anticipation of the examples, consider a multivariate time series consisting of a set of P time series $x_p(t)$ with $1 \leq p \leq P$. These series are assumed to be time aligned with N samples, that is, $t = 0, 1, \dots, N - 1$, and to represent (individually) samples of a second-order stationary process.

As above, begin by computing the multitaper eigencoefficients

$$\hat{x}_{k,p}(f) = d_{k,p}(f) \sum_{t=0}^{N-1} x_p(t) v_t^{(k)} e^{-i2\pi ft} \quad (19)$$

where the $d_{k,p}(f)$ are the adaptive weights (see [54, Sec. V] for details). When the spectrum is white, the weights $d_{k,p}(f) = \sqrt{\lambda_k}$ and so the weights are approximately unity for $k < K$.

To estimate the spectral matrix, one first collects the weighted eigencoefficients (19) into a $K \times P$ complex matrix

$$\mathbf{X}(f) = \begin{bmatrix} \hat{x}_{0,1}(f) & & \hat{x}_{0,P}(f) \\ \vdots & \dots & \vdots \\ \hat{x}_{K-1,1}(f) & & \hat{x}_{K-1,P}(f) \end{bmatrix} \quad (20)$$

so the formal estimate of the $P \times P$ spectral matrix $\hat{\mathbf{S}}(f)$ is

$$\hat{\mathbf{S}}(f) = \frac{1}{K} \mathbf{X}^\dagger(f) \mathbf{X}(f) \quad (21)$$

where the \dagger represents a conjugate transpose. Here, again, there has been a change from the theory (and what practice there was) of Wiener’s 1930 “Generalized Harmonic Analysis” [11] through to modern texts, e.g., [74] and [75] where the spectral matrix plays a central role. Our experience is that one rarely computes $\hat{\mathbf{S}}(f)$ directly but usually the diagonal elements (power spectra of the individual series), coherences and phases (often with jackknife error estimates), or takes the singular value decomposition (SVD) of $\mathbf{X}(f)$. Some examples are shown later.

Due to the superior spectral leakage properties of the multitaper spectrum, Fig. 3 demonstrates why one should go to this effort. It shows the minimum, average, and maximum of eight multitaper (MT) spectra made on nonoverlapping ~ 3 h blocks with a periodogram computed on the first block. Over most of the frequency range the periodogram is biased by at least a factor of 1000, a large error. Below ~ 35 mHz, the ratio of the maximum to minimum of the eight MT estimates varies between ~ 100 and ~ 500 , not the ~ 3.5 that one would expect from Hartley’s “maximum F -ratio” [76] indicating reasonable nonstationarity during the day. Above ~ 35 mHz the average spectrum is close to that expected from quantization noise $\sim 9.1 \times 10^{-6}$ Pa²/Hz, and near the expected range.

A. Multivariate Analysis and Likelihood

One should note that beginning with the matrix $\mathbf{X}(f)$, or its many variants, one can apply most of the standard methods of multivariate analysis with some minor differences. First, the usual column of “ones” is missing; second, the matrices are all functions of frequency; and third, everything is complex valued, so “Gaussian” and “normal” are not synonymous. In compensation, there is a long history showing that Fourier transforms of “reasonable” data have an approximately Gaussian distribution, so tests such as Bartlett’s “ M ” that are often avoided because of their sensitivity to departures from Gaussian, work quite well.

We assume the process is “locally white,” that is, that the true spectrum is approximately constant on $(f - W, f + W)$, the rows of $\mathbf{X}(f)$ are approximately uncorrelated, and $\hat{\mathbf{S}}(f)$ will have a complex Wishart distribution with $2K$ DoF. For the matrix to be nonsingular, one must have $K > P$. For scalar series the spectrum estimates are distributed as χ_{2K}^2 , are

approximately unbiased, and are approximately maximum likelihood [77].

If one collects the eigencoefficients (17) into a vector

$$\mathbf{Y}(f) = [y_0(f), y_1(f), \dots, y_{K-1}(f)]^T \quad (22)$$

its covariance matrix

$$\mathbf{C} = \mathbf{E} \{ \mathbf{Y}(f) \mathbf{Y}^\dagger(f) \} \quad (23)$$

whose elements may be evaluated using the spectral representation

$$\mathbf{C}_{jk} = \int_{-\frac{1}{2}}^{\frac{1}{2}} S(f - \xi) \mathcal{V}_j(\xi) \mathcal{V}_k^*(\xi) d\xi. \quad (24)$$

The concentration of the Slepian functions implies that one may replace the integral over $[-(1/2), (1/2)]$ with one over $(-W, W)$ with negligible error

$$\mathbf{C}_{jk}(f) \approx \int_{-W}^W S_o(f - \xi) \mathcal{V}_j(\xi) \mathcal{V}_k^*(\xi) d\xi. \quad (25)$$

This means that one can test for specific shapes in the spectrum, that is, $\hat{\mathbf{S}}(f)$ is proportional to $S_o(f)$ in the range $(f - W, f + W)$, with log-likelihood

$$\mathcal{L}(f; S_o) = \ln |\mathbf{C}| + \mathbf{Y}^\dagger(f) \mathbf{C}^{-1} \mathbf{Y}. \quad (26)$$

In the bandlimited approximation, the eigenvalues of $\mathbf{C}(f)$ are the eigenvalues of the corresponding Karhunen–Loève expansion.

VIII. PERIODICITY, THE HARMONIC-F TEST, AND T^2 TESTS

Generally speaking, harmonic analysis has come to mean the study of the line components in a spectrum without regard to whether they are at multiples of a common frequency. Unfortunately, since the techniques used for harmonic analysis have been virtually identical to those used for general spectrum estimation, the two names have been used almost interchangeably. The distinction, however, is crucial because it has been shown that one cannot specify both the spectrum and

first-order probability density arbitrarily [78]. In other words, the periodic components should be considered to be part of the mean-value function, not of the random part.

To make sense of harmonic analysis, it is essential to recognize that the assumption of “pure” line components is a convenient fiction, while often good for a moderate time span is rarely supportable over extended periods of time. This tends to further divide the subject by series length: in short series, detection and resolution of line components are major problems; for longer series, the problems of interest typically concern the structure of the line; that is, could it be the result of a high-Q resonator driven by noise, or is it a sinusoid with time-varying amplitude or frequency or both? In cases where there is barely enough data to make a detection, such distinctions are often ignored but, as the length and precision of data increases, so does the necessity of careful analysis.

In our applications, we invariably assume that frequency is continuous because the frequencies that appear in data are determined by nature and do not depend on the choice of sampling interval or the size of the sample. Thus, the conventional Fourier frequencies (those spaced $1/N$) are more-or-less irrelevant and one must zero pad the data, use a “slow” Fourier transform [79], or interpolate the eigencoefficients. (And even here, polynomial interpolation error formulas imply that the process is much more accurate if one zero pads by a factor of π or better before interpolating.) Experience is a hard teacher and we have learned to keep frequencies in Hertz—using a mixture of cycles/hour, cycles/day, etc., makes it all too easy to miss noting common frequencies in different data series.³

Multitaper analysis [54] approached the problem of “mixed” spectra, that is, where line components are embedded in stationary background noise with a continuous spectrum, using a regression approach. The method described below extends this to multivariate and cyclostationary problems. With this approach, which consists simply of applying regression techniques to the eigencoefficients [54], the two problems of spectrum estimation and harmonic analysis are distinct. There is also no distinction between an ordinary constant mean and periodic components except for the trivial one that, in real-valued data, there are only half the DoF for the constant mean.

The distinction between the two problems is that spectrum analysis is the study of the second and higher moments of $dX(\nu)$ while the emphasis in harmonic analysis is on the first moment of $dX(\nu)$, effectively a Munk–Hasselmann [80] extension of the spectral

representation. In such cases, the process is usually described as having a nonzero mean value function consisting of a number of sinusoidal terms at various frequencies, plus perhaps a polynomial trend, plus a stationary random process of the type we have been considering in Section VI. In terms of the spectral representation this, in practice, amounts to having

$$\mathbf{E}\{dX(f)\} = \sum \mu_m \delta(f - f_m) df \quad (27)$$

in place of the usual assumption $\mathbf{E}\{dX(f)\} = 0$. With this definition, the continuous portion of the spectrum is the second absolute central moment of $dX(f)$.

A. The Harmonic F-Test

To show the derivation for the harmonic F-test, assume the simplest case of a single line component at frequency f_0 so that the eigencoefficients have a nonzero expected value

$$\mathbf{E}\{y_k(f)\} = \mu V_k(f - f_0). \quad (28)$$

Again making the assumption that the continuous component of the spectrum near f_0 is slowly varying or “locally white” (25) shows that

$$\text{Cov}\{y_k(f), y_j^*(f)\} \approx S(f) \cdot \delta_{j,k} \quad (29)$$

where the spectrum $S(f)$ is the continuous spectrum and does not include the line power.

There are two obvious limiting methods to estimate μ : point regression at f_0 and integral regression in the neighborhood of f_0 with the obvious changes to either both coefficient weighting. The second case (integral regression) is more complex, and as it uses information from a wider bandwidth, it is subject to noise from the same bandwidth. For this reason, point regression is more commonly used. In this (first) case, one uses only the data at f_0 where one has the obvious relation

$$\mathbf{E}\{y_k(f_0)\} = \mu V_k(0) \quad (30)$$

and can estimate the mean μ by standard complex regression methods [81]

$$\hat{\mu}(f) = \frac{\sum_{k=0}^{K-1} V_k(0) y_k(f)}{\sum_{k=0}^{K-1} V_k^2(0)}. \quad (31)$$

³We makes an exception for paleoclimates where the time step may be in millennia.

This estimate is the high resolution estimate described in [54, Sec. 10] at $f = f_0$ before squaring. As the eigencoefficients are combined linearly we may write

$$\hat{\mu}(f) = \sum_{n=0}^{N-1} h_n(N, W) x_n e^{-i2\pi f(n-\frac{N-1}{2})} \quad (32)$$

where the effective harmonic analysis data window $h_n(N, W)$ is given by

$$h_n(N, W) = \frac{\sum_{k=0}^{K-1} V_k(0) v_n^{(k)}(N, W)}{\sum_{k=0}^{K-1} V_k^2(0)}. \quad (33)$$

The variance of the estimated mean depends on the local continuous part of the spectrum

$$\text{Var}\{\hat{\mu}(f)\} = \frac{S(f)}{\sum_{k=0}^{K-1} V_k^2(0)} \quad (34)$$

which is only slightly larger than $S(f)/N$. Subtracting their estimated means from the eigencoefficients gives an estimate of the continuous spectrum. Comparing this value of the background spectra with the power in the line component results in an F variance-ratio test [82], [83], with 2 and $2K - 2$ DoF for the significance of the estimated line component

$$F(f) = \frac{(K-1)|\hat{\mu}(f)|^2 \sum_{k=0}^{K-1} V_k(0)^2}{\sum_{k=0}^{K-1} |y_k(f) - \hat{\mu}(f)V_k(0)|^2}. \quad (35)$$

B. Comments on Significance Testing

When applied to climate data or data from some process correlated with climate, it is common for the harmonic F -test to produce an unusual number of lines at intermediate significance levels. With monthly or economic data, one must beware of “calendar frequencies” produced by the irregular lengths of the months [84]. These aside, the spacing between lines can provide useful information.

As an example, the Burgundy grape harvest series [14] beginning in 1370, records the day of the year when Pinot Noir grapes were harvested in the vicinity of Dijon and is of importance because it is both the longest such series and particularly because it includes a long span of observations before the Maunder minimum. It was found that this interval, noted for a long span with no sunspots and “the little ice age,” also marked a change in the spectrum of the grape harvest data [85] at about 1675. Taking the entire span of 634 years with $C_R = 4$ and $K = 5$, the

F -test found one frequency, 0.2412 c/y (a period of 4.146 \pm 0.0022 years) with a significance of 99.9%.

The Pinot Noir series has a total of 49 frequencies in the F -test with significances above the 90% level. Ten percent of 634 suggests that these may be simply random noise but looking at their spacings one finds: 13 pairs with an average spacing of 18.63 years, close to the lunar nodal period of 18.613 years; 16 pairs spaced by 103.9 years, the Suess cycle from ^{14}C . This agrees well with a period between 103.97 and 104.14 years in [62]; 18 pairs spaced 80.02 years. The period of the Gleissberg cycle was given as 80 years [86], but estimates vary; see [87]; 23 pairs spaced an average of 53.79 years, the McKenzie cycle first identified in 1829 in English wheat prices [88]; and 19 pairs at an average spacing of 34.98 years, possibly the second harmonic of the Suess cycle.

It seems unlikely that, if the frequencies were random, one would get these numbers of pairs of equally spaced differences and adding the fact that they correspond to known solar and climate periods, we are inclined to the opinion that the climate is responding to a complicated forcing mechanism. However, as noted in [62], many of these periodic components do not appear as “additive periodicities,” but as modulations of the statistical structure of the process. Moreover, there are enough long periods in the climate system that shorter period terms may be modulated by the longer period components so the F -test will be suppressed. The annual temperature cycle can be offset from the tropical year by precession and phase modulated by the solar cycle; see [89]. The lesson here is that, when working with long data series, do not expect to find behavior that mimics simple models.

C. Common Periodic Components and the T^2 Test

Turning now to the periodic components with lower amplitudes, one suspects that these consist of a mixture of solar rotation (that varies between ~ 25 days at the Sun’s equator to ~ 40 days at its poles) and related geometric effects, convection modes [34], [90], [91], possibly gravity (g) modes [92] or their aliases, and possibly unknown effects. Our object here is not to identify specific sources on the Sun so, for simplicity, we refer to all of these as simply “lines.”

When considering a multivariate series of this type, at a line frequency the eigencoefficients will be the complex line amplitude times the value of the corresponding Slepian Function at zero frequency. Thus, returning to the derivation in Section VII, one expects that the columns of (20) will have a mean value given by the zero-frequency Slepian function. That is, if series p contains a term at frequency f_m so that

$$x_p(t) = a_{p,m} \cos(2\pi f_m t + \theta_{p,m}) + \dots \quad (36)$$

the corresponding eigencoefficient at a frequency f close to f_m will have an expected value

$$\mathbf{E}\{y_{k,p}(f)\} = \frac{a_{p,m}}{2} e^{i\theta_{p,m}} V_k(f - f_m). \quad (37)$$

Because the $V_k(f)$'s are very small for $|f| > W$ one can usually treat lines separated by more than W as being independent.

Denote by \mathbf{V} the $K \times 1$ vector of $\{V_k(0)\}$'s and by $\mathbf{A}(f)$ the $P \times 1$ vector of complex amplitudes $a/2 \exp\{i\theta\}$ and write

$$\mathbf{X}(f) = \mathbf{V}\mathbf{A}^T(f) + \mathbf{R}(f). \quad (38)$$

One now estimates $\mathbf{A}(f)$ by ordinary (complex) least squares at each frequency on a fine mesh and, at each frequency, we can test the fit for significance using a complex T^2 statistic [93]. Formally, one computes the unnormalized residual spectrum

$$\mathbf{S}_R(f) = \mathbf{R}^\dagger(f)\mathbf{R}(f) \quad (39)$$

$$T^2(f) = \|\mathbf{V}\|^2 \frac{K-P}{P} \mathbf{A}^\dagger(f) \mathbf{S}_R^{-1}(f) \mathbf{A}(f) \quad (40)$$

but, in practice, one reduces $\mathbf{R}(f)$ with a QR decomposition in the usual way. $T^2(f)$ has an F distribution with $2P$ and $2(K-P)$ DoF; see [94]. With a single series this test becomes the usual harmonic F -test derived in the previous section, and many of its properties are similar.

If one chooses the point \hat{f} , where the harmonic F -test is maximized as an estimate of line frequency, its variance is

$$\text{Var}\{\hat{f}\} = \frac{1}{(2\pi T)^2} \frac{6}{\rho(f)} \quad (41)$$

where, as above, T is the total length of the series and $\rho(f)$ is the local signal-to-noise power ratio. Other things remaining constant, the variance of the frequency estimate decreases as $1/T^3$ so the accuracy of a frequency estimate can be much better than the Rayleigh resolution. This implies that one must zero pad extensively or zero pad by π and interpolate.

To close this section on periodic components we reiterate the point [78] that one cannot specify both the spectrum and the first-order probability density independently. Experiments where one sets the significance level of the harmonic F -test, subtracts the estimated lines from the time-domain data, and plots a histogram of these residuals have favored relatively low thresholds, that is, most of the data we have been studying have many lines.

A related procedure is to note that multitaper estimates have a χ_ν^2 distribution, where ν is the DoF at frequencies where lines are absent, but the presence of line components causes the distribution to be noncentral $\chi_{\nu,\lambda}^2$, where λ is the noncentrality parameter, the sum of squares of the periodic or modal components [36]. The signal-to-noise power ratio $\rho = \lambda/\nu$. The distinction between the central and noncentral components has become increasingly important with big data sets because, once one has long enough data sets to resolve the various periodic and modal components, a spectrum estimate has a mixture distribution; noncentral at modes and central between them. Examples are given in [19, Plates 2–6] and [36, Figs. 5 and 6].

IX. ROBUST ESTIMATES: HOW MUCH IS TOO MUCH?

Since Box's introduction [95] of the term “robust” into the statistics literature in 1953, the field has exploded and searching on “robust statistics” in Google Scholar produced a staggering 2.8 million hits. Having contributed several papers to this literature ourselves (see, e.g., [5], [6], [53], [96]–[102]), we have both a vested interest but, also having been subjected to large quantities of seismic, geomagnetic, and space physics data, one begins to wonder if robustness was not “oversold.” In Sections X-C and X-D, we examine two examples of robust time series analysis and find: first, that the “median spectrum” commonly used in seismic noise studies can be seriously misleading; and second, the common practice of clipping extreme data may result in incorrect inferences about processes generating much data.

A. The Median Spectrum

To frame the discussion of the properties of the frequently used median spectrum, we will start with the procedures used to study seismic “hum” and seismic noise, e.g., [15] and [22]. In Section X-D, the artifacts resulting from the median spectrum are demonstrated with specific data examples. The robust variant of the Welch Spectrum estimation procedure used in [15] and [22] is as follows.

- 1) Choose a block length from one to four or five days duration. This choice governs the frequency resolution of the estimate, and a block of duration T seconds will correspond to a Rayleigh resolution $\mathcal{R} = 1/T$. A one-day block will have a resolution $\mathcal{R} = 11.57 \mu\text{Hz}$. The data blocks are usually offset by 50% of their duration and often skip intervals after large earthquakes. Assume that there are J blocks, and label the successive blocks by j with $1 \leq j \leq J$. Let N denote the number of data samples in a block. Standardize the sampling interval to $\delta t = 1$, and denote the data (possibly after removal of the local average, slope, and known effects such as tides) in the j th block by $X_j(t)$ with $t = 0, 1, \dots, N-1$.

- 2) Taper the data on each block with a Hamming or better data taper $D(t)$, and compute the spectrum estimates

$$\hat{S}_j(f) = \left| \sum_{t=0}^{N-1} D(t) X_j(t) e^{-i2\pi ft} \right|^2. \quad (42)$$

- 3) In each frequency bin in the selected frequency range, sort the J estimates into increasing order

$$\hat{S}_{(1)}(f) \leq \hat{S}_{(2)}(f) \leq \dots \leq \hat{S}_{(J)}(f) \quad (43)$$

using the common statistical notation that a subscript (j) denotes the ordered values. Keep the median $\hat{S}_{(J/2)}(f)$ as the estimate. The motivation for this procedure is that one expects normal modes excited by large earthquakes to occur in the upper quantiles $\sim \hat{S}_{(\lesssim J)}(f)$ and the median excludes them.

There are dangers with such a procedure. First, for such problems the median has an efficiency of only $\sim 48\%$, meaning that its variance is twice that of an efficient estimator, so assessing effects such as temporal dependence is unnecessarily difficult. Second, the estimate is biased. This does not prevent identifying modes, but the estimated power in the modes will be low by a factor of ≈ 1.35 . This complicates the identification of forcing mechanisms. Third, the series may be nonstationary causing misidentification of peak frequencies in median spectrum.

To establish the baseline performance of this procedure we assume that the data are approximately a Gaussian colored noise process as one expects from resonances driven by turbulence. We also assume that, apart from large earthquakes or other outliers occurring in some blocks, the process is stationary. The individual spectrum estimates (42) will have a central chi-square distribution with two DoF, that is

$$z_j(f) = \frac{\hat{S}_j(f)}{\mathbf{E}\{\hat{S}_j(f)\}} \quad (44)$$

will have the probability density function e^{-z} . In (44), the expected value $\mathbf{E}\{\}$ of the estimate is

$$\mathbf{E}\{\hat{S}_j(f)\} = \int_{-\frac{1}{2}}^{\frac{1}{2}} |\tilde{D}(\xi)|^2 S(f - \xi) d\xi \quad (45)$$

where $S(f)$ is the true spectrum of the process at frequency f and $\tilde{D}(f)$ is the Fourier transform of the data taper $D(t)$. Robust spectrum estimates from such distributions have been studied previously [5], [6], [53], for general choices of the clipping level, and in [19], general χ^2_{2K} distributions were considered. Many of the problems occur because most of our experience with robustness is from symmetric distributions, and the exponential distribution is emphatically not symmetric.

B. A Robust Spectrum Estimate

Consider a set of J independent variates z_j from a standard exponential distribution $\exp\{-z\}$, with a population mean of one, that is, $\mathbf{E}\{z_j\} = 1$. The z_j 's are sorted into increasing order

$$z_{(1)} \leq \dots \leq z_{(j)} \leq \dots \leq z_{(J)}. \quad (46)$$

Properties of the order statistics of the exponential distribution are available in Volume 2 of [103, p. 500], and the expected value, or mean, of the j th quantile is

$$\mathbf{E}\{z_{(j)}\} = \mathcal{M}_j(j) = \sum_{m=1}^j \frac{1}{J+1-m} \quad (47)$$

for $1 \leq j \leq J$. This means that if one repeats the experiment of taking J independent variates and keeps the j th smallest sample from each experiment, they will have the mean $\mathcal{M}_j(j)$ and variance

$$\mathbf{Var}\{z_{(j)}\} = \sum_{m=1}^j \frac{1}{(J+1-m)^2}. \quad (48)$$

For $j = 1$, (47) gives $\mathbf{E}\{z_{(1)}\} = 1/J$ and, for $j = J$, one has

$$\mathbf{E}\{z_{(J)}\} = \sum_{m=1}^J \frac{1}{m} \approx \ln J + \gamma + \frac{1}{2J} \quad (49)$$

where $\gamma = 0.57721566\dots$ is Euler's constant. That is, one expects the smallest and largest values in a random sample to be $1/J$ and $\sim \ln 1.78J$, respectively. We associate these order statistics with the probabilities

$$P_j = 1 - e^{-\mathcal{M}_j(j)}. \quad (50)$$

Fig. 4 shows the expected values of the order statistics from a sample of size $J = 100$ independent exponential

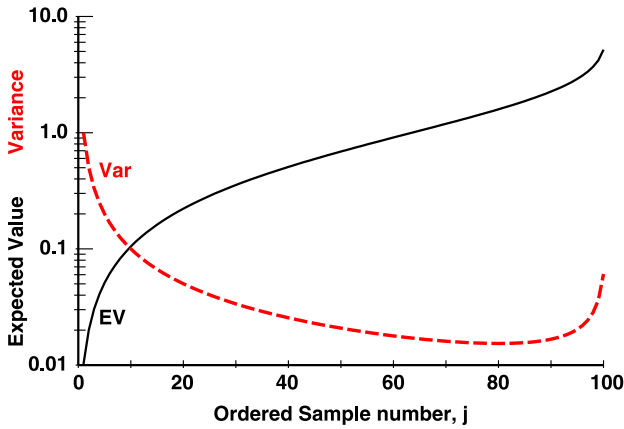


Fig. 4. The solid black line shows the expected value \mathcal{M}_j of the order statistics of a sample of size $J = 100$ independent exponential variates. The red dashed line shows the variance $\mathcal{V}_{100}(j)$ of the unbiased estimate (52).

variates and it can be seen that the lowest ten have expected values that are a factor of 10–100 below the mean of 1. Similarly, the top 15 are factors of 2–5 larger than the mean. This bias can be corrected by defining a gain factor

$$\mathcal{G}_j = \frac{1}{\mathcal{M}_j(j)} \quad (51)$$

so the estimated mean, say $\hat{U}_{[j]}$, from the j th order statistic

$$\hat{U}_{[j]} = \mathcal{G}_j \cdot z_{(j)} \quad (52)$$

is unbiased, but the $\hat{U}_{[j]}$'s are not monotone. Within the expected statistical fluctuations, all values of j should give an unbiased estimate of the spectrum. The variance of $\hat{U}_{[j]}$, scaling (48) by the squared gain, is

$$\mathcal{V}_{(j)} = \text{Var}\{\hat{U}_{[j]}\} = \mathcal{G}_j^2 \text{Var}\{z_{(j)}\}. \quad (53)$$

The DoF of $\hat{U}_{[j]}(f)$ can be estimated from the first two moments of a chi-squared distribution $\hat{\nu} = 2/\mathcal{V}_{(j)}$ to set approximate confidence intervals. Returning to the example with $J = 100$, the red dashed line in Fig. 4 shows the variance of the unbiased estimates as a function of j so both small and large quantiles should be avoided. For an uncontaminated sample, the minimum variance (maximum-likelihood) estimate is the arithmetic mean of the z_j 's with a variance of $1/J$ or 0.01 in this case. Thus, none of the single quantile estimates is particularly

efficient. The median has an efficiency of $\sim 48\%$ and the minimum variance 0.0154 (an efficiency of 65%) occurs at $j = 80$. Also note that one cannot simply average the various $\hat{U}_{[j]}$'s and obtain a much better estimate because the sorting causes them to be correlated. Estimates that use a linear combination of all the variates $z_{(j)}$, up to some limit, say $J' < J$, are discussed in [5] and [6]. Finally, the spectra discussed in the remainder of the paper are all computed with sections overlapping by 50% and so are clearly not independent. For a noise-like process, the correlation between these spectra on adjacent sections (see [5, Sec. 3.3]) is only 3.33%.

X. LARGE-SCALE DATA EXAMPLES

The previous three sections have discussed the multitaper spectral analysis techniques and their applications and implications for “big data” sets. In this section, we will present results from signals originating in the Sun, which working out from the Sun are observed by interplanetary spacecraft, geomagnetic observatories, and by finally at terrestrial seismic stations. In addition, we observe artifacts of these solar signals in long duration surface temperature records. Before doing this, however, we define four families of normal modes, two solar and two terrestrial, that are referred to in the following section. The distinction is important because all four of these families are observed in terrestrial seismic data.

A. Solar and Terrestrial Normal Modes

Modes are usually described by a spherical harmonic expansion and consequently have a set of “quantum numbers” l , n , and m . Here l represents the spherical harmonic degree and gives the number of nodal lines in latitude. The radial order n is the number of zeroes along a radial line. Finally, m gives the azimuthal order, that is, the number of cycles in longitude with $-l \leq m \leq +l$. Except where necessary, we omit the m index.

The solar modes of interest here are the *pressure* (p -modes) and potentially *gravity* (g -modes), denoted as $p_{l,n,m}$ and $g_{l,n,m}$, respectively. Introductions to helioseismology are given in [104] and [105].

Pressure or p -modes are acoustic standing waves in the frequency range $\sim 250 \mu\text{Hz}$ to $\gtrsim 5000 \mu\text{Hz}$, so their periods range from about an hour down to a few minutes. Their frequencies are given asymptotically by

$$\nu_{l,n,m} \asymp \nu_r \cdot m + \nu_0 \left[\frac{1}{2} \left(l + \frac{1}{2} \right) + n + \alpha \right] + \dots \quad (54)$$

where $\nu_0 \approx 135 \mu\text{Hz}$ and the rotational splitting term ν_r is approximately 440 nHz, but depends on the particular mode. The solar p -modes are split into $2l + 1$ singlets, indexed by $-l \leq m \leq +l$. The lowest frequency p -mode

$p_{0,1}$ has a predicted frequency of $\sim 258 \mu\text{Hz}$, but very few p -modes have been definitively observed. The frequencies of p -modes vary slightly with solar activity [43], and this variation is larger at the upper end of the p -mode band than it is at lower frequencies.

Solar buoyancy, or gravity, or g -modes arise from a density inversion at the top of the solar core. They have frequencies $\lesssim 500 \mu\text{Hz}$, but the consensus is that they have not been identified in the sense of assigning quantum numbers.

Solar p -modes have been detected in charged particles and the interplanetary magnetic field in space [18], in terrestrial data [21], and others cited in [32, Sec. 7]. Line frequencies corresponding to predictions of solar g -modes were reported in [18] and in terrestrial seismic data in [34, Sec. XXI].

Terrestrial seismic S - and T -modes are well described in several texts, e.g., [106, Ch. 8] or, for details, [27]. Briefly, spheroidal modes are denoted by ${}_nS_l$, and toroidal modes by ${}_nT_l$. Tables of mode frequencies and Q 's are given in [28] and further discussion in [16].

B. Spectral Indices of Interplanetary Magnetic Fields

The nature of turbulence and evolution of the solar wind with radial distance from the Sun has been studied since the dawn of the space age. Numerous studies have concluded that, on average, the spectral index denoted by G , that is, the slope of the spectrum measured on a log-power versus log-frequency setup is approximately $5/3$, that is, the spectrum can be described approximately as

$$S(f) \approx \frac{S_1}{f^{5/3}}. \quad (55)$$

In the solar wind, this does not hold at either very low or very high frequencies; see [107, Fig. 1]. Strictly speaking one should use wave number k rather than frequency f , but in most cases, suitable data are not available and it is commonly assumed that wave number is proportional to frequency. The index $-5/3$ is generally taken as a signature of Kolmogorov turbulence and its presence in power spectra of solar wind data has been taken as evidence that the solar wind is turbulent. We emphasize that we do not question this observation (e.g., [21, Fig. 1]), but rather its interpretation.

Despite the many papers on turbulence in the solar wind there are problems. First, almost all the papers in this field select data intervals conditioned on, for example, the speed of the solar wind [108], visual inspection [109], etc. As a result they violate the conditions stated in the quote by Airy given in Section X-C or, in modern terms, suffer from selection bias. Second, Kolmogorov turbulence is a stationary process. However, given evidence for solar wind anisotropy conditioned on the

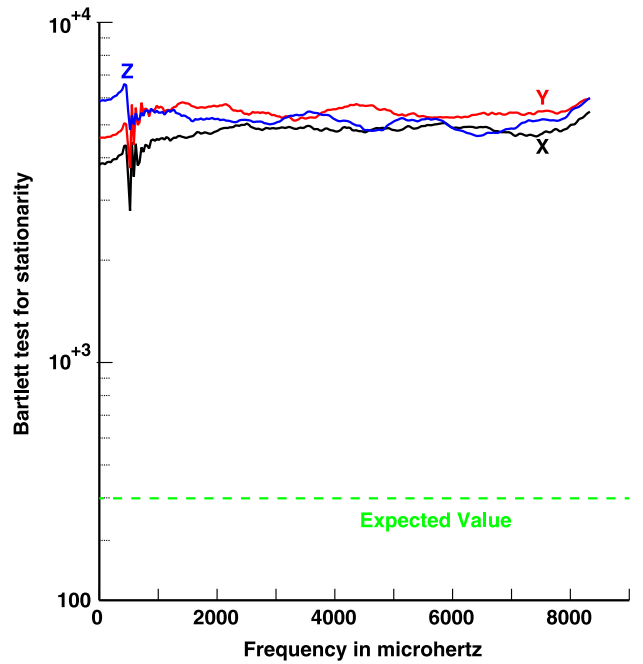


Fig. 5. The Bartlett test for stationarity applied to 400 sections of ACE IMF data. In these tests, 3-h data blocks (180 1-min samples) offset by 6 h were used. The spectrum on each block was computed using $K = 10$ Slepian tapers with a time bandwidth of $C_R = 5.5$. The test was performed on all three components separately with that for B_x in black, B_y in red, and B_z in blue, defined in GSE coordinates. For a stationary process, one expects a χ^2_{399} distribution. The test levels, 5000, show that stationarity is not a tenable assumption.

magnetic field [110], plus the implicit recognition of nonstationarity in the selection bias problem, solar wind turbulence must be questioned. Fig. 5 shows the results of a simple data analysis experiment where spectra computed on 400 blocks of IMF data from the ACE spacecraft during 1999 were estimated and compared. Each block was 3 h long with a 3-h gap between blocks. At an average solar wind speed of 500 km/s these blocks are separated by over five million kilometers. Each spectrum was estimated with $C_R = 5.5$ and $K = 10$. The comparison used Bartlett's M -statistic; see [111, Table 32] or [6, Sec. IV]. When the process is stationary, this test has an approximately chi-squared distribution that with 400 data blocks has ~ 399 DoF. For all three components [X , Y , and Z in geocentric solar ecliptic (GSE) coordinates] $M \sim 5000$, so stationarity must be strongly rejected. The break at $\sim 250 \mu\text{Hz}$ is near the transition from g - to p -modes.

Thus, observed statistical properties exclude Kolmogorov turbulence as an adequate explanation for fluctuations in the solar wind. This makes most studies of radial evolution of solar wind turbulence invalid because, if one does not understand the physics causing nonstationarity, one cannot select data sections from a

nonstationary process and then pretend that the results have general validity.

1) *Data Analysis Experiments*: Following up on this, we tried the following experiment. First, take fixed-length blocks of interplanetary data, compute a spectrum on each block, and estimate the slope (in a log-frequency–log-power frame) on each block. Following [109], we began with 3-h blocks of ACE IMF data. These were offset by 1 h and computed every hour for a year. Fig. 6 shows multitaper spectra from two adjacent, but nonoverlapping, blocks, and it can be seen that the indices differ dramatically.

Second, regard the series of slopes as a new time series and compute its spectrum. This is found to have many low-frequency, high-Q peaks. The spectra from the 3-h blocks showed signs of being aliased and the peaks appear to correspond to solar g-modes, similar to the results in [37]. The frequency range of solar g-modes is limited to $\lesssim 400 \mu\text{Hz}$ corresponding to a sampling rate of 20 min.

Third, we used 45-min data blocks offset by 20 min. However, instead of working with a single component of the magnetic field, we took all three components. To partially compensate for an obvious nonstationarity, the magnetic field components from the Ulysses spacecraft were multiplied by its heliographic radius. We computed the eigencoefficients (here with $C_R = 4.5$ and $K = 8$), formed matrices (20), found their singular value

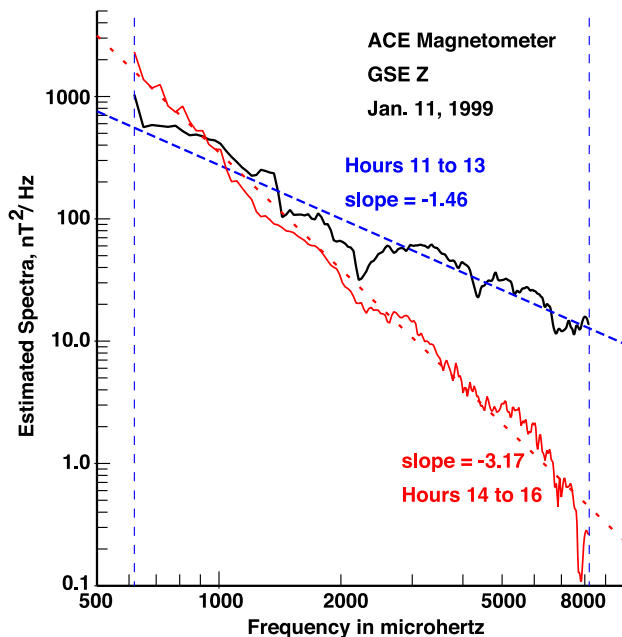


Fig. 6. Two spectra of the GSE B_2 component of the IMF at ACE for hours 11 to 13 (black) and hours 14 to 16 (red) on January 11, 1999. The estimated slopes, shown by dashed lines, are 1.46 and 3.17, respectively.

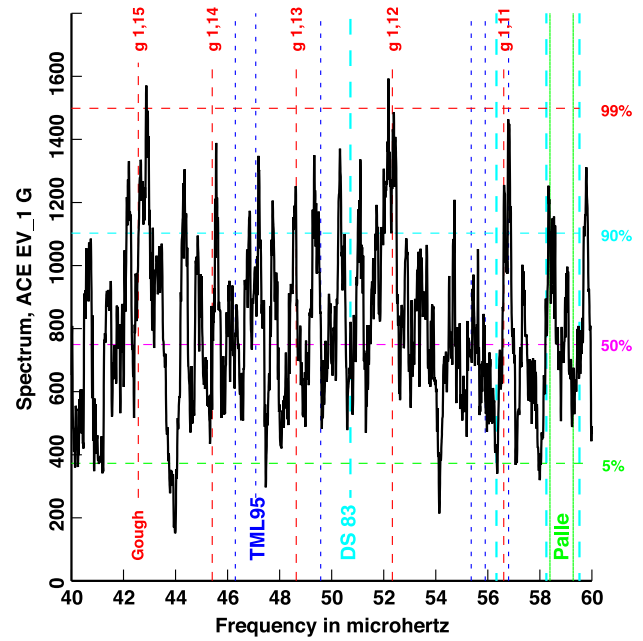


Fig. 7. Spectrum from ACE $\vec{B} : G^{[1]}(t)$. Spectrum days 1–365, 1999. Resolution: 32 nHz, $C_R = 5$, $K = 8$. Proposed observations of solar g-modes: blue [18]; cyan [112]; green [113]. Theoretical solar g-mode frequencies (red), D. Gough (personal communication).

decomposition (SVD), and replaced the spectrum with the eigenvalues when estimating the index. We refer to the spectral index of the largest eigenvalue as $G^{[1]}(t)$.

Fourth, Fig. 7 shows a power spectrum of $G^{[1]}(t)$ for 1999. The spectrum has been postwhitened and the peaks show reasonable agreement with some possible measurements of solar g-modes [18], [112], [113] and theory.⁴

Fifth, Fig. 8 shows a comparison between ACE and Ulysses. There was an approximate radial alignment of ACE and Ulysses in 1999. Sixty days of data were used, giving a low-resolution spectrum. However, as may be seen in Fig. 8, there is remarkable agreement between the two spectra. Scaling the Ulysses data by radius (≈ 5.08 to 4.99 AU during this interval) does not change the slope. There is a reasonably sharp small cutoff, $\sim 290 - 300 \mu\text{Hz}$ in the spectrum near the edge of the g-mode band, but closer to the transition between g-modes and p-modes. Given the low resolution, the “index spectra” at ACE and Ulysses are nearly identical. This implies that, with 1-min data and between 0.99 and 5.2 AU, the statistics of the slopes do not evolve detectably. Taking a longer 299 day block between 2003 day 271 and 2004 day 205 when Ulysses was near aphelion and between heliographic latitudes of $\pm 7.6^\circ$ (chosen to have the same range as Earth and ACE), the average index was -2.218 at ACE and -2.203 at Ulysses. The minimum index among the 27000 samples was

⁴D. Gough, personal communication.

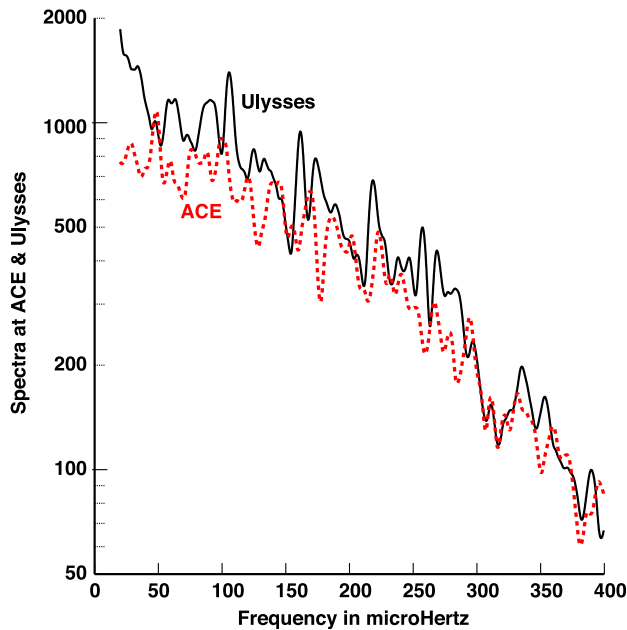


Fig. 8. Spectral index data ACE: DOY 42–102, 1999, Uly: DOY 60–110, 1999, (4320 samples, $\delta t = 20$ min) $C_R = 5$, $K = 8$ windows. Note that there are no corrections for the different orbits. There are only minor changes in the spectra. Solar p -modes have a frequency range $\sim 250 \mu\text{Hz}$ to $\gtrsim 5000 \mu\text{Hz}$. Solar g -modes theoretically have frequencies $\lesssim 500 \mu\text{Hz}$.

below -5.1 for both spacecraft while the standard deviation increased from 0.583 for ACE to 0.775 for Ulysses.

How does one explain these observations? The histograms of the indices appear similar at both spacecraft with only minor evidence for evolution between 0.99 and 5 AU, and the difference may depend on their necessarily different distribution of heliographic latitudes sampled. The distribution at Ulysses is nearly uniform, but U-shaped at ACE. However, spectra of the index series had a larger modal component at Ulysses than that observed at ACE.

A possible sequence of events to explain the observations is to begin in the turbulent solar convection zone. It has high densities, high temperatures, is completely ionized, has strong magnetic fields, supersonic flows, high conductivities, low damping, and generally everything that is required to generate Kolmogorov turbulence. The convection zone turbulence drives both p - and g -modes. This is a standard assumption and agrees with theory by [114] and the observation that signal-to-noise ratios of modes in the IMF is approximately constant across frequency. Proceeding outward, both turbulence and modes drive surface phenomena and modulate the solar wind by the same mechanism.

Magnetic field lines and particles flow radially outward from the Sun as originally proposed in [115] and [116]. A combination of horizontal flows and g -modes

(whose surface motion is mostly horizontal) moves the footprint of the flux tubes in an apparently random manner. The seismic surface of the Sun is ~ 300 km below the photospheric surface [117], so most interface phenomena are not directly observable. However, our hypothesis is that the $f^{-5/3}$ baseline observed in spectra of interplanetary data is a fossil remnant of the convection-zone turbulence.

On longer time scales, one sees the average position of flux tubes and analyzing long series shows solar modes as the dominant phenomena. Most, $\gtrsim 99\%$ of the energy in the IMF occurs in the g -mode band, that is, at frequencies $< 500 \mu\text{Hz}$, so given the observation that magnetic fields control anisotropy in the solar wind [110], evolution of the spectral index may depend on the magnetic signatures of g -modes. Given the relatively stronger modal characteristics of data at Ulysses compared to those on ACE (but lower overall power), one wonders if the presence of modes does not, in fact, suppress turbulence.

Also note that these ideas should be considered preliminary and that they push both ends of the spectrum estimation problem. The short blocks cause some bias on the index estimates, whereas taking a year or so of these index estimates runs into many of the same resolution problems as other helioseismology problems, so improvements are needed in both.

C. Geomagnetism and Robustness

Fluctuations in Earth’s geomagnetic field induces currents on electrical cables, pipelines, and similar structures and can cause overheating in power system transformers, corrosion on pipelines, and power supply problems in communications systems; e.g., see [118] and [119]. The problem is not new, and was first documented by Barlow in 1849 [120].

A persistent problem in attempting to analyze geomagnetically induced currents (GICs) and in the closely related field of magnetotellurics [121] is that the effective signal-to-noise ratio is inexplicably poor, outliers are common, and large amounts of data are often needed. Estimating the induced voltage on a cable from fluctuations in the geomagnetic field requires transfer functions. Estimating these transfer functions [121] is often unsatisfactory because the estimates are excessively variable across frequency and the residuals from the frequency-domain regressions are often much larger than seems reasonable. The variation across frequency was pronounced on Transatlantic cables [122], and a cepstrum [58] gave a delay of 110 min. The source of this apparent delay is unknown. The high residuals appearing in transfer function estimates are the result of coherences between magnetic fields and GICs from cables being “improper.” This means that if $E_k(f)$ denotes the eigencoefficients of the induced electric field at some frequency f and $B_k(f)$, the corresponding ones for a

component of the magnetic field, the “improper” (or reverse) cross-spectrum $\sum_k E_k(f)B_k(f)$ is often larger in magnitude than the “proper” (or forward) cross-spectrum $\sum_k E_k^*(f)B_k(f)$ where the superscript * denotes complex conjugate. See the discussion in [123]. Moreover, the improper terms are often distributed across the frequency spectrum and so form a “noise source” whose power is similar or larger to that in the proper components. Again, however, the source of the improper data is not well understood and it was only recognized recently [17].

In addition to these effects, time series of geomagnetic or interplanetary magnetic fields commonly have periods of quiescence interspersed with intervals of high activity and it has been common practice to classify these into “quiet” and “active” days since at least the 1860s. Fig. 9 shows a plot of moving quantiles from the East component of the geomagnetic field at Eskdalemuir, Scotland and the effect is obvious. However, it has been recognized for almost as long that this traditional classification, while convenient for many purposes, is not scientific and, in 1863 [124], G.B. Airy, the Astronomer Royal, stressed

First, that there is no such thing as a day really free from disturbance, and no reason in the nature of things for separating one or more days from the general series. There is abundant reason for such separation on the grounds of convenience, etc. Under these circumstances, I cannot think it right that I should cut off a part of that salience, with the belief of obtaining results that can possess any philosophical value, from the part which is left.

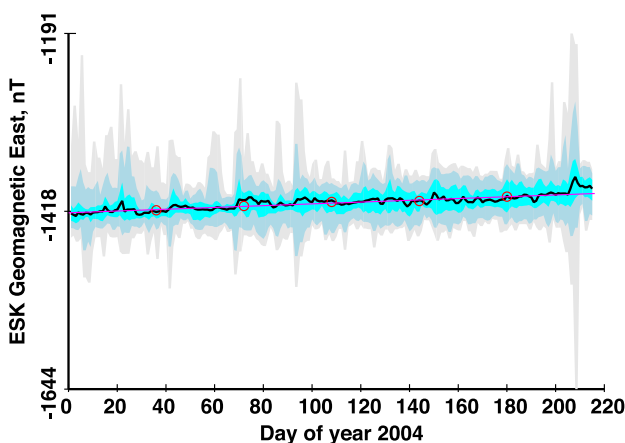


Fig. 9. Summary plot for a relatively short section, 215 days, of the East component of the geomagnetic field at Eskdalemuir. Here $\Delta t = 240$ s, and summary statistics are computed on two-day blocks (720 samples), offset 50%. The bands shows minimum-to-maximum, light gray; 5% to 95%, blue-gray; and 25% to 75%, cyan, with the median in black. The red line is a linear trend.

While recognizing the propensity for outliers to occur in many kinds of data, most of the robust procedures do exactly what Airy is warning against and “cut off part of that salience.” However, one must also recognize that much data are not Gaussian and that large “salience” in data do not imply that the data have been contaminated or have incorrect samples. A few extreme cases of large impulsive transient events such as lightning strikes and the like are real physical signals. On the other hand, one of the largest effects on an estimated spectrum from an outlier in our experience is shown in [6, Figs. 12 and 18]. This was a true error, a repeated data sample, almost invisible on an ordinary data plot, but it did produce an error $\gtrsim 10^7$ across much of the frequency range. It was also not an extreme, so one must be very careful not to confuse extreme values with contamination.

As a simple experiment we took data recorded by the Boulder, CO, USA geomagnetic observatory from January 30, 2002 to March 15, 2004, low-pass filtered and decimated to $\delta t = 5$ min. We stress that there is nothing unusual about the Boulder data; indeed it appears to be a very well-run observatory. Different time intervals and data from other well-run observatories give similar results (see Fig. 9), and our impression is that there are no indications of instrument malfunction or data contamination and the extremes are an accurate portrayal of the state of the geomagnetic field.

Given these data, we computed a robust (Winsorized) scale with the lower and upper 10% of the values trimmed. As an example, on the X (North) component the ordinary standard deviation is $\sqrt{\mu_2} = 25.165$ nT, the kurtosis $\beta_2 = \mu_4/\mu_2^2 \approx 54.5$, and the robust scale $\hat{\sigma}_w \approx 20.846$ nT. Fig. 10 shows the time-of-day dependency for extremes greater than $\pm 15\sigma$ for the North and Vertical components as a function of time-of-day over an extended interval, January 1999 to May 2009. There are significant differences in patterns but both imply strongly cyclostationary behavior. Extremes on the Eastward, or Y, component are both fewer and closer to having a uniform distribution in time-of-day and are omitted.

We then varied the clip point c from 3σ to 50σ , replacing points outside $\pm c\hat{\sigma}_w$ with a linear interpolation. Next, we computed spectra and F -tests on ten 100-day blocks with a 25-day overlap. A time-bandwidth product $C_R = 6$ with $K = 10$ tapers was used. Finally, we computed the number of peaks in the harmonic F -test, $F(f)$ with the results shown in Fig. 11. The point of this plot is that simple clipping peaks reduce the number of potential periodic components from nearly 6000 with no clipping to just under 4000 with clipping at 3σ .

At high significance levels there are many more peaks in these spectra than one can reasonably account for by chance [36]. Randomly permuting the order of the data (see [36, Fig. 6 and Table 2]) gives crossing rates that agree with Gaussian theory. Because the original and

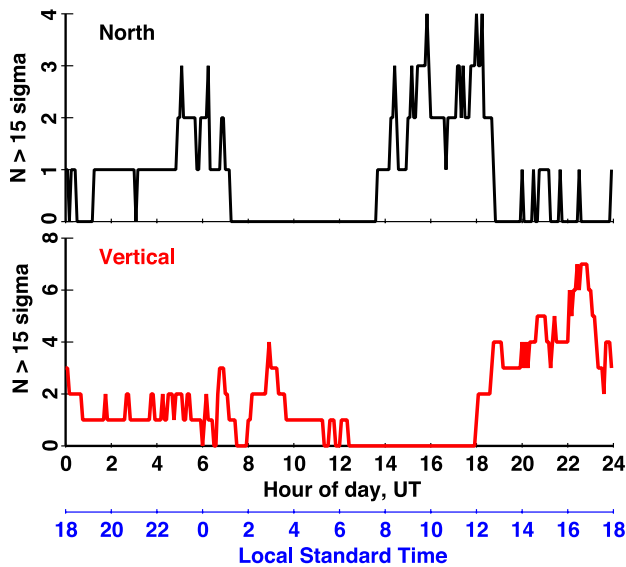


Fig. 10. Time-of-day dependency for extremes larger than 15σ for the North (top, black) and Vertical (lower red) in Boulder geomagnetic data.

permuted data have identical first-order probability distributions, we conclude that the large number of peaks observed depends on the temporal order of the data and not its amplitude distribution. Similar effects have been observed in charged particles and magnetic fields in interplanetary space [18], [19]; in data from the ACE spacecraft at the first Lagrange point L_1 [36], [125]; in geomagnetic fields recorded at other observatories; and in the solid earth [16]. The only explanation that we have found for the number, frequencies, and Qs of these peaks is that they originate as normal modes of the Sun. Observed on Earth, these modes are further split by

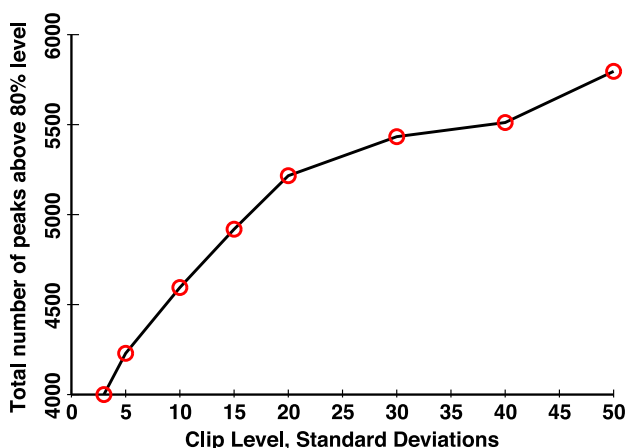


Fig. 11. Number of peaks in the harmonic F-test in the three components of Boulder, CO, USA geomagnetic data as a function of the time-domain clip level.

Earth’s rotation and in all cases must be corrected for the orbit of the observing instrument (including the Earth) around the Sun.

The fact that more peaks are found as the clipping level is increased has another major implication; namely that the peaks in the time-domain data are a result of the modes, and are not just “outliers.” That is to say many of the large peaks seen in such data occur when several modes become phase aligned. This is analogous to a “Dirac comb” where a sequence of periodically spaced impulses in the time-domain has a Fourier transform that is also a periodic series of impulses in the frequency domain. Low-frequency solar modes are not equally spaced in frequency so this is not an exact analogy, but extremes are perhaps best described informally as “several modes becoming phase aligned.” Similar effects are common in wideband amplifiers where phase alignment of the various subchannels causes the amplifier to saturate. The Sun does not appear to have a similar power limitation.

D. Seismic Spectra

The low-frequency seismic noise spectrum, particularly of the horizontal components, is enigmatic. Here we discuss two contributing factors to these problems. The first is statistical, specifically, bias and other problems associated with the procedures commonly used as discussed in Section IX-A. The second is physical and it appears that much of the problem in understanding horizontal seismic data is that the solar contribution is relatively strong at low frequencies. In [126], it is noted that the seismic hum on the horizontal components is not explained by ocean forcing. Solar modal signals are often larger than the median and often are the strongest signals present. Given that the Sun is the source of these signals, one must consider their characteristics, and Stix notes [105, p. 183] that

The general appearance is that “one-third oscillates”—either of a given area at any one time, or of a given period of time at any one location on the solar surface; but this pattern changes continuously.

While obviously not a precise mathematical description of any particular mode, such observational insight should not be ignored. Also remember that this is based on ordinary solar p -modes in the 2–5-mHz band and the low-frequency modes may be different. Signals that are present 1/3 of the time will usually be missed by a procedure that expects them to be present 1/2 of the time.

1) *Black Forest Observatory Example:* The problem with seismic data is that all of the properties predicted in Section IX-A are violated. To illustrate this, we used the North velocity from the STS-1 instrument at Black Forest Observatory (BFO) between January 10 and July 4, 2004. This was globally a seismic quiet period

with only two earthquakes with $M \geq 7$ and 49 with $M \geq 6$ distributed over the 157 day interval. The horizontal components of the STS-1 are known to be insensitive to magnetic fields [127], so the solar peaks in the spectra cannot be from geomagnetic coupling to the instrument. For seismic normal mode frequencies, we use [28] augmented with singlet frequencies provided by Masters (the $2l+1$ singlets of low-frequency seismic modes can occupy a band nearly $20 \mu\text{Hz}$ wide; see [27, Table 14.1].) For solar p -mode theory we used [50] and, for the few measured solar p -modes below 1 mHz, [128]. These are denoted $p_{l,n}$.

The data were prewhitened and our initial experiment was with 350 24-h blocks. Each section had its average and linear trend subtracted and a single NW = 2 Slepian taper applied, see [34, Sec. V.B]. We then fit a quadratic to $\ln \hat{S}_{(50\%)}(f)$ over the band 150–1250 μHz and removed the fit from all $J = 350$ order statistics. The median spectrum (Fig. 12) is less variable (across frequency) than expected and much less so than the spectra made from either the 20% or 80% levels. Looking at statistics across the 200–1200- μHz band, Fig. 13 shows that the average increases gradually with quantile up to about the 90% level after which it increases rapidly. Similarly, the variance divided by the expected variance (53) drops slightly initially, and again increases rapidly after about the 80% point. Finally, the ratio of the maximum to average spectrum shows a roughly U-shaped blue curve as a function of frequency. The behavior at the upper end of these curves is not explained by the few $M \gtrsim 6.5$ earthquakes and both the low end and the behavior in the 80%–90% range is enigmatic. Exploratory studies suggest that the seismic noise has several components: the lowest quantiles, <10% or 20%, may just be thermal noise (but see below); between 20%

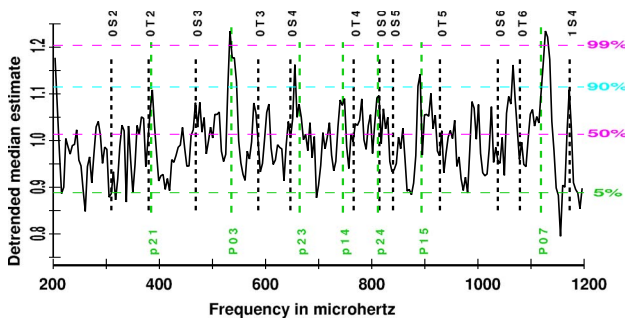


Fig. 12. Detrended median spectrum of 350 sections of BFO-North using 24-h blocks. Horizontal dashed lines show 5%, 50%, 90%, and 99% significance levels based on the chi-squared approximation. Green vertical dashed lines show observed solar p -mode frequencies. Black vertical dashed lines show observed terrestrial S - and T -mode frequencies. Only two peaks exceed the 99% significance level, at 533 and 1127 μHz , both within one-quarter of a Rayleigh resolution ($\mathcal{R}/4$) of the measured p -modes $P_{0,3}$ and $P_{0,7}$, respectively.

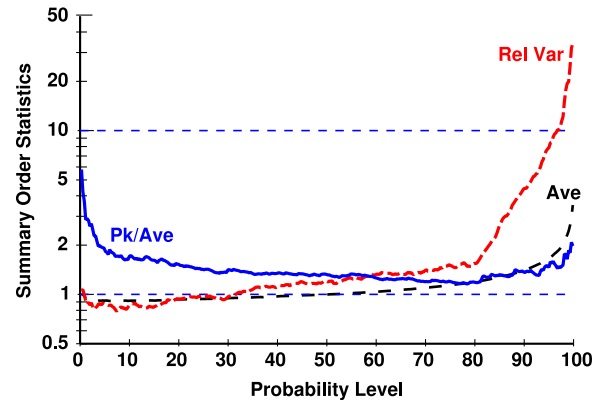


Fig. 13. Observed statistics of 350 24-h spectra of BFO-N seismic velocity. The black dashed line shows the average order statistics. The red dashed line shows the variance divided by the expected variance. The blue solid line shows the ratio of the maximum to the average spectrum. Blue dashed horizontal lines show the 1% and 10% order statistics.

and $\sim 50\%$ there is reasonable correlation with the planetary K_p index; above that there are earthquakes and discrete solar modes. That is, the data are stratified. Moreover, the seasonal dependence of the three lower components appears to vary in different ways, but this needs considerable further study. In particular, the median spectrum (Fig. 12) has several moderate peaks that superficially appear to be at the frequencies of the Earth’s normal S and T modes, but on closer examination, they are not.

We estimated robust autocorrelations between the spectrum estimates on consecutive blocks for each frequency. Significant correlations were observed out to delays in excess of 35 days and we examined the largest ones carefully. Of these only one, the 24th largest, at $f = 1037.60 \mu\text{Hz}$ and $\tau = 7$ days, was close to a seismic normal mode ${}_0S_6$ at $1037.55 \mu\text{Hz}$. This is also close to the measured frequency of the solar $P_{1,6}$ mode at $1039.65 \mu\text{Hz}$. Solar p -modes are expected to be split into $2l+1$ singlets spaced $\sim 0.45 \mu\text{Hz}$ apart, so these frequency comparisons cannot be better than a few μHz .) Averaged over delays, the highest correlation occurred at $723.27 \mu\text{Hz}$, $0.4\mathcal{R}$ from the predicted frequency of $p_{3,3}$ at $718.39 \mu\text{Hz}$. Twenty of the largest 100 autocorrelations occur within $\pm(1/2)\mathcal{R}$ of this mode at delays from $\tau = 1.5$ to 21 days. Excluding ${}_0S_0$ (at $812.838 \mu\text{Hz}$), seismic modes damp much faster than this.

To improve frequency resolution, we computed the spectra on 83 sections, each 100 h long, offset by 50 h. This was zero padded to 32k giving a frequency increment of $0.254 \mu\text{Hz}$. Unbiased quantile estimates for the 20%, 50%, 80%, 90%, and 100% (the maximum) levels were computed and a quadratic fit made to $\ln\{U_{50\%}(f)\}$ over the band 150–1250 μHz . This fit was removed from all estimates. Fig. 14 shows the flattened spectra over

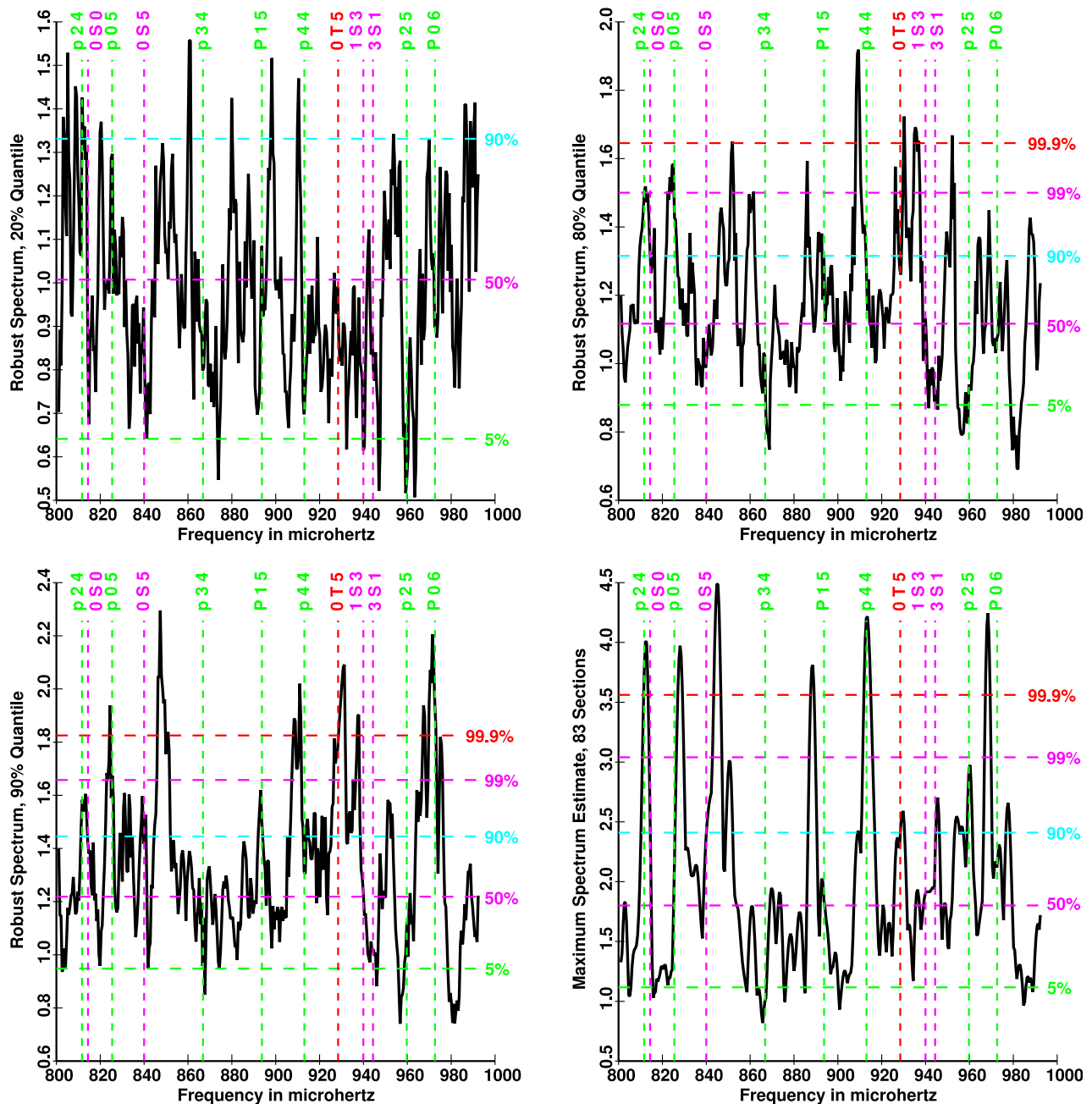


Fig. 14. Four unbiased [in the sense of (52)] and detrended spectrum estimates from 83 100-h blocks of the BFO North data, corresponding to the 20%, 80%, 90%, and 100%, or maximum. The horizontal dashed lines show significance levels based on the chi-squared approximation. The vertical dashed lines indicate the frequencies of solar p-modes in green, and seismic S and T modes in magenta and red, respectively. Note that many of the largest peaks in the 90% and 100% estimates agree with solar, not seismic, normal modes. Many of the other peaks agree with solar mode frequencies offset by ± 1 c/d, or with higher l modes. As shown in Fig. 13, the average level creeps up with quantile. Also, the peak frequency varies with quantile, implying that these estimates do not give reliable frequency estimates.

800–1000 μHz . Several things are apparent. First, the difference in character between the four estimates implies that, as with the one-day blocks, the estimates are not stable. The median to 90% curves have over 80 DoF (Table 1), so their standard deviations are about 0.16 and the differences between the curves are much

larger than this. Second, comparing the median curve with Fig. 12, one goes from two peaks just over the 99% level to many above the 99.9% level. Third, the peak frequencies vary between levels. There were nine cases where two of the five estimates were on the same FFT bin, but only two cases with three such

Table 1 Theoretical Quantities Associated With the $J = 83$ Section Spectra. The 20%, 80%, 90%, and Max Entries are Shown in Fig. 14. In 83 Spectrum Estimates the Largest (Bottom Line) Is Expected to be 5.0021 Times the Mean and so Is Scaled by 0.1999. In Stationary Gaussian Data This Estimate Will Have a Variance of 0.0653 Times the Mean Spectrum Squared, Corresponding to 30.6446 DoF

j	Mean $\mathcal{M}_{83}(j)$	Gain \mathcal{G}_j	Variance $\mathcal{V}_{83}(j)$	DoF	Prob. %	Notes
1	0.0120	83.0000	1.0000	2.0000	1.20	Min
17	0.2276	4.3929	0.0591	33.8541	20.36	20%
42	0.6991	1.4303	0.0248	80.6629	50.30	Med.
67	1.6213	0.6168	0.0185	108.1528	80.24	80%
75	2.2842	0.4378	0.0202	98.8784	89.81	90%
83	5.0021	0.1999	0.0653	30.6446	99.33	Max.

agreements. Fourth, it appears that several of the peaks agree with seismic mode frequencies. Some of these agreements are summarized in Table 2 for those cases where a) the peaks exceed the 99.9% significance level and b) the observed peak agrees within $\pm(1/2)\mathcal{R}$ ($\pm 1.39 \mu\text{Hz}$) of an identified solar or seismic mode. We also allowed splittings of 1 cycle/day on solar modes [34].

Of the 20 peaks identified in Table 2, 16 are seismic. The problem is that only three of these occur when earthquakes with moment $> 10^{26}$ dyne-cm occur within or closely before the data block. Moreover, if one looks at the maximum spectrum from the 83 blocks, many of the solar peaks are larger than nearby peaks at seismic mode frequencies.

Table 2 Matches Within $\pm(1/2)\mathcal{R}$ Between Peaks in Spectra and Known Modes. For Solar P -Modes the ± 1 Denotes a ± 1 Cycle/Day Offset. On Seismic S and T Modes the Third Index Is m . The Columns Marked f_{th} and f_{obs} Are the Known and Observed Peak Frequencies, “Sid” the Spectrum Quantile, and “doy” the Day in 2004 Where the Maximum Occurred. Those Marked With a “*” Have Earthquakes With Moment $> 10^{26}$ Dyne-cm Within the Segment

f_{th}	mode	f_{obs}	Sid	doy
246.4	$P_{0,1} - 1$	245.7	90	133
269.5	$P_{0,1} + 1$	270.1	max	33
300.0	${}_0S_{2,-2}$	300.1	90	22
391.3	$P_{0,2} - 1$	391.1	max	33
464.3	${}_0S_{3,-2}$	463.4	90	20
470.9	${}_0S_{3,+1}$	470.9	90	31
583.3	${}_0T_{3,-3}$	583.4	80	*39
587.6	${}_0T_{3,0}$	587.5	90	183
644.8	${}_0S_{4,-2}$	644.4	max	*39
651.3	${}_0S_{4,+4}$	651.6	80	137
674.1	${}_1S_{2,-2}$	674.4	80	120
677.7	${}_1S_{2,-1}$	677.0	50	91
768.1	${}_0T_{4,+1}$	768.0	max	14
812.8	${}_0S_0$	812.3	80	*116
926.2	${}_0T_{5,-5}$	926.2	80	110
930.1	${}_0T_{5,+5}$	930.3	80	106
930.9	${}_0T_{5,+2}$	931.3	90	110
1034.5	${}_0S_{6,-6}$	1034.5	max	16
1079.1	${}_0T_{6,-4}$	1079.3	80	183
1130.2	$P_{0,7} + 1$	1130.2	50	*116

Fig. 15 shows standardized quantiles $\hat{U}_{ij}(f)$ for solar and seismic modes that occur reasonably close in frequency, are both clearly visible in Fig. 14, but have quite different characteristics. The seismic ${}_0T_{5,0}$ mode (the last subscript indicating the $m = 0$ singlet) is centered at $f = 930.551 \mu\text{Hz}$ and the spectrum is above the 99.99% significance level on the 90% quantile but is relatively small on the maximum. However, none of the spectral peaks in its frequency range appear to be closely associated with known earthquakes (see Table 2). This mode has 11 singlets distributed somewhat unevenly between 926.239 and 930.944 μHz , a range that appears to include the solar $P_{9,3}$ mode at 930.540 μHz [129], so the 19 singlets of this mode will cover a range ~ 926.9 to $\sim 934.1 \mu\text{Hz}$. Thus, the frequency range covered by the singlets of $P_{9,3}$ overlap those of ${}_0T_5$. The solar $P_{0,6}$ mode at $f = 972.61 \mu\text{Hz}$ [130], in contrast, is the largest on the maximum. The closest seismic modes are ${}_2S_{2,2}$ at 955.542 μHz and ${}_0S_{6,-6}$ at 1014.526 μHz well outside the bandwidth of the spectrum estimation procedure. Returning to Fig. 15, one observes that for probabilities in the 15%–55% range behavior for both modes is similar and biased slightly low, probably indicating a need to use a more robust fitting procedure to determine the overall baseline. Below the median, ${}_0T_5$ behaves about as expected, and the general increase in level above the median may be due to the numerous $M \gtrsim 6$ earthquakes and occasional coupling to solar modes. The

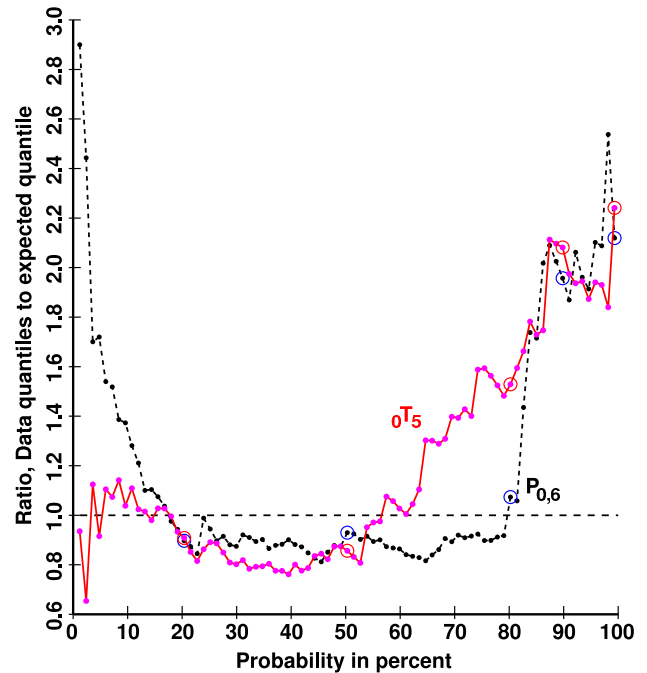


Fig. 15. Standardized quantiles $\hat{S}_{ij}(f)\mathcal{G}_j(j)$ versus P_j for the solar $P_{0,6}$ mode at $f = 972.61 \mu\text{Hz}$ (black) and the seismic ${}_0T_5$ mode at $f = 930.55 \mu\text{Hz}$ (red). These modes are reasonably close in frequency and both are prominent in Fig. 14.

lower peak in the $P_{0.6}$ curve suggests that there is always some signal present. The sharp increase beginning around 80% appears to be a reflection of the “one-third oscillates” phenomena modulated by the Earth’s orbit and the general seasonal dependence of geomagnetic activity.

2) *Discussion—Median Spectrum:* We have shown that medians of power spectrum estimates done on short blocks are both biased and inefficient. Correcting for the bias one finds that the average varies with the quantile. Moreover, at many frequencies, the spectrum estimates are highly correlated over durations of 20 days and more. Worse, the procedure appears to miss most of the significant low-frequency features in the data. Taking 100-h data segments we found many peaks significant above the 99.9% level in the BFO North seismic velocity. The frequencies of these peaks correspond closely to those of solar normal modes and not those of the normal modes of the Earth. In several cases, these peaks are higher than nearby peaks at seismic mode frequencies. These spectral peaks are narrow, implying that they are being driven by a high- Q (> 1000) source. Their detectability varies with quantile, suggesting that the data consist of a mixture of processes with approximately stratified amplitudes. This implies that this analysis method should be used cautiously at low frequencies.

Looking again at Fig. 14, the differences between the estimates are almost as large as in Figure 16 of Kay and Marple’s 1981 comparison of spectrum estimates [131]. Here, even though quantile estimates are “Min-Max” [132], the differences seen between the different quantile estimates are striking. Although the median estimate was chosen to exclude the effects of large earthquakes and the data interval contains a $M > 7$ earthquake, the largest peaks in the spectrum appear to be solar. Thus, we stress that, when computing spectra from large quantities of data, use more than one estimate, understand the properties of the different estimation procedures, and plan for the unexpected.

E. Daily Temperature

Recently, several excellent long series of daily European weather records [133] have become available and, to make the examples easier, we analyze some of them here. The series are summarized in Table 3. All of these series were preprocessed in the manner discussed at the

Table 3 Long Daily European Temperature Series. The First and Last Years Are Given Plus the Initial Julian Ephemeris Day Number (JD_s) and the Number of Samples (N)

City	Start	End	JD_s	N
Padua	1774	1996	2369001.0	81449
Stockholm	1756	1998	2362426.0	88754
Uppsala	1722	1998	2350019.0	101161

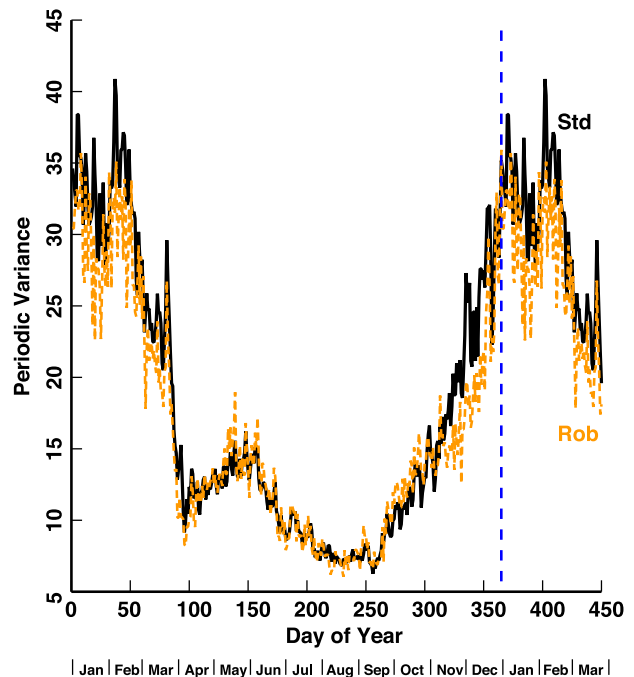


Fig. 16. Periodic Variance for the Uppsala daily temperature data. The solid black curve is ordinary variance; the dashed orange is a robust estimate. Note the “discontinuity” near day 80, the vernal equinox.

end of Section VIII-A, and the harmonic T^2 - and F - tests were computed.

The Uppsala series of daily temperatures [134] has the distinction of being the longest one that exists. It begins on Monday, January 12, 1722 and continues to the present. In total, it is just over 100000 samples so easily handled as a single block.

Such data are cyclostationary with a period of one year. In the Uppsala data the period appears to be indistinguishable from the Gregorian calendar year, but again with long data spans this must be tested, not assumed; see [89], [135], and [136].

We begin by removing the annual temperature cycle. The variance (Fig. 16) was initially computed on a 1461-day

Table 4 Statistics of Cyclostationary Magnitude-Squared-Coherence Between Uppsala Daily Temperature at f and $f + 1$ cycle/year. Left Column Is Significance (Fraction of Frequencies Above Level and Number of Local Maxima Above Level) in Randomly Permuted and Original Data, $N = 101, 161$

Prob., %	Randomly Permuted		Original Data	
	%	Peaks	%	Peaks
90.	9.641	4454	59.859	18673
99.	1.039	533	25.787	8735
99.9	0.157	95	8.918	3270
99.99	0.012	11	2.600	1016
99.999	0.001	1	0.700	314
99.9999	0.000	0	0.115	52

“year” to account for leap years, then averaged down for plotting. There are two estimates, the ordinary variance estimate and a robust [137] estimate. There is little difference, confirming the impression that the data quality is excellent. There is, however, a change of about 6:1 in variance over the year and, strangely, a “discontinuity” near the vernal equinox. This implies that the data will be strongly cyclostationary (or periodically correlated). Such processes are discussed in [100] and [138] and in the recent book [139].

If one now computes the dual-frequency magnitude-squared coherence (MSC) [99], [139] between frequencies f and $f + 1$ cycle/year, one finds 8735 local maxima above the 99% significance level. For this reason, it does not appear to be possible to scale the data to remove the coherence between frequencies. Overall, about 25.8% of the estimates are above the nominal 99% level showing highly significant coherence. As shown in Table 4, randomly permuting the temporal order of the residuals and repeating the operation results in 533 local maxima with 1.04% of the frequency range above the 99% level, close to expected. Fig. 17 plots the lowest 300 nHz of this coherence (about 20 pages of such plots would be required to cover the Nyquist bandwidth) and some remarks are in order. First, the large peak near the center is the first harmonic to the Rieger periodicity (154-day, ~ 75.15 nHz), found in 0.3–100-MeV solar gamma rays [140]. Second, the plot demonstrates a common problem that one finds in most of these long data sets, namely

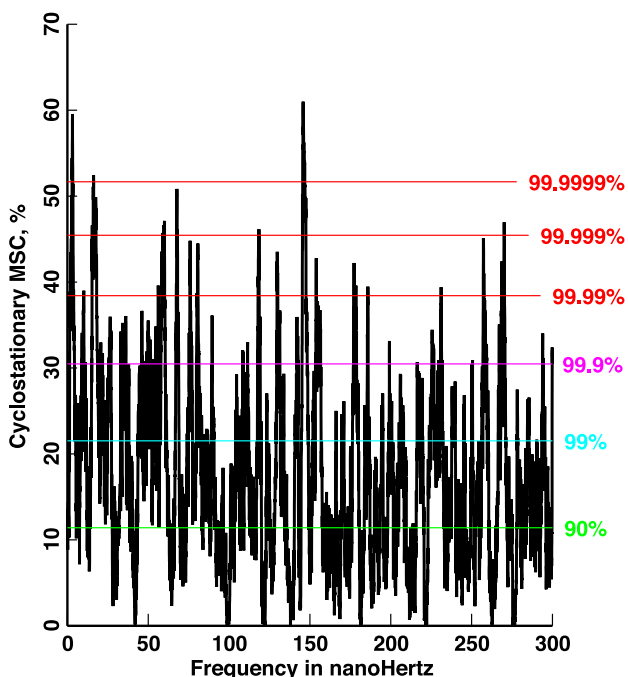


Fig. 17. Cyclostationary MSC between the Uppsala data at frequency f and $f + 1$ c/y. Horizontal colored lines delineate significance levels based on the chi-squared approximation.

that the MSC estimates are almost bimodal, high at modal frequencies, and low at noise levels between peaks. This may be seen even more clearly in the following plot where the frequency range is 3 nHz instead of 300.

Because at least some of these peaks in the real data have the same frequencies as measured in interplanetary space [18], it can be assumed that there may be a few thousand low-level solar modes contributing to the temperature variance. One assumes that, in the daily temperature data, most of these are aliases of g-modes. These modes are split by Earth’s orbit and so can be detected at f and $f + 1$ cycles/year (c/y). We have begun a study of this general topic in [34], but much work remains to be done. Suitable data are usually not available and analysis methods are being developed simultaneously with applications. One problem is that of time scales, and in examples such as the dropped-call rate in cellular phone systems operating near 900 MHz [141] much of the problem is solar. Engineers are used to acquiring data, but when the fundamental periods causing the problems range from hours to decades, data spans of years may be required. This causes problems because changes in systems occur too frequently to ensure a homogeneous data stream.

In both cases, the problem is that one has many low-amplitude periodic components at (usually) unknown frequencies and these will result in apparent coherent behavior whenever f_1 and f_2 correspond to line frequencies. A Loève spectrum [54] of the Uppsala data may well contain $\sim (8735)^2$ peaks above the 99% level. This is misleading because periodic components should be considered part of the mean-value function, not the second moments, and mixing the two leads to confusion. However, the 25.8% of the MSCs above the 99% significance level implies that either the continuum spectrum is also significantly coherent or that the spectrum is almost “all lines.” The line problem can be partly solved with the complex T^2 -test discussed in Section VIII-C. A possible solution to the continuum problem is discussed in [39].

Fig. 18 shows a harmonic T^2 -test for common periodic terms in daily temperature data at Stockholm [142] and Padua [143]. The data begin in 1774 and end in 1993, a span of 220 years. (The annual cycle from both series was removed before further processing and a few outliers in the Padua series from the early 1940s were interpolated.) Here a relatively high time-bandwidth product $NW = 11$ with $K = 20$ tapers was used, so spectra have ~ 40 DoF. The plotted frequency range, 1.108–1.111 μHz , with a total bandwidth of 3 nHz was chosen to include the 1.11- μHz line detected in interplanetary electrons by the HISCALE detector [144] on the Ulysses spacecraft [18]. This peak exceeds the 99.9999% significance level and has an estimated synodic frequency of $\approx 1.10951 \mu\text{Hz}$. Even with ~ 100000 samples, a peak at this significance level would be unusual. This agreement between sidereal and synodic frequencies implies that the mode has azimuthal order of $m = 0$. The detection of this

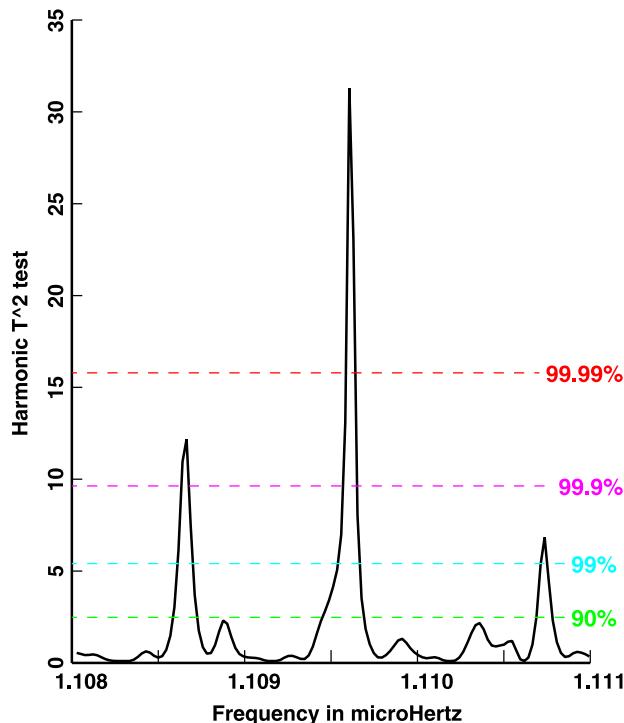


Fig. 18. Harmonic T^2 test for common periodicities in the daily temperature series at Stockholm and Padua. The record spans 1774 to 1993 giving a Rayleigh resolution of 114 pHz. In this test, the frequency was prespecified from Ulysses spacecraft data. The estimated common frequency is $\hat{f} \approx 1.10951 \mu\text{Hz}$, corresponding to a synodic period of ≈ 10.4317 days.

peak in both interplanetary data and terrestrial temperature appears to answer the question posed in [145]. There are 8735 peaks where the cyclostationary MSC at f and $f + 1$ c/y exceed the 99% level, and a large fraction of these also have high values of T^2 .

Again, the lessons contained in this short section are that climate data are complicated, and intimately linked to the Sun. It is cyclostationary, and contains many solar modes—there are about 1.5 lines per nHz, and at least some of them can be identified with known solar effects.

XI. SUMMARY AND CONCLUSION

In this paper, we have sketched some of the things learned in work with climate, geomagnetic, interplanetary, and seismic data. These data sets, with literally thousands of time series, are mostly long; just one set of seismic data has 122 records ranging from short ones, 60 days duration with only 51 million observations to several with over 100 million samples, and an extraordinary few with unbroken seismic data extending over 400 days. The climate data considered here, in contrast, have a much smaller number of samples, only about 100000 daily samples, but spanning nearly 300 years. The geomagnetic and space data are intermediate sized

with sampling rates lower than they are for seismic data, but long, almost unbroken series are more common. The distinction is important: in seismic data some of the data breaks are to recenter the mass, which disrupts the continuity of signal and introduces artifacts. Since connecting adjacent sections without introducing low-frequency artifacts can be tricky, we have mostly chosen to operate with long continuous stretches. With spacecraft data, in contrast, data gaps are often from communications problems and so are easily interpolated. We are not sure if such data count as “big” or not. However, we can testify that visually scanning a data set that extends over years or decades for problems certainly makes it seem like a lot. Even worse, examining a spectrum or coherence estimated from such a data set is a major task. As we have shown, most such estimates made from long data sets show thousands of solar modes or peaks offset from known solar modes by multiples of a cycle/day, a cycle/year, or both. Smoothing such estimates simply confuses the issue and usually just results in a plot that is “wrong everywhere”—it neither shows the high modal peaks nor the low intervals between modes.

Very few, if any, of these series can be considered to be independent. One sees coupling between data taken in interplanetary space, in ground-based magnetometers, and on to seismic data. It seems that all data measured on Earth are influenced by the normal modes of the Sun. This changes how we must think about such data. Previously, one would have considered the “noise”—generally including the things that we cannot control or do not understand—to be independent between sensors spaced by modest distances in either time or space. This is probably true for the preamplifier noise in the instruments, but not for other background fluctuations in air temperature or pressure, geomagnetic, or seismic noise, and one expects the list to grow.

Compounding this problem, we have also shown that robust statistical procedures have, perhaps, been overdone and can be misleading when there is not good evidence for outliers. Other data, such as the series of spectral indices from the ACE spacecraft push spectrum estimation methods to all its limits. One used to take some comfort in the idea that spectrum estimates would be asymptotically unbiased and that, if one could just get a long enough span of data, all the problems would disappear. This has turned out to be complete nonsense; we now have very large data sets, the analysis of which has not become simpler as a result of their enormity. In fact, the scientific implications of big data such as the geomagnetic spectral index analysis here, instead of confirming our intuitive notions of turbulence, show that solar turbulence dynamics are rather poorly understood.⁵ So

⁵Reading the introduction to *Mathematics 596—An Introduction to the Frequency Analysis of Time Series* by John W. Tukey [146, pp. 503–506] and other papers in this volume and [147] gives much insight into the departures between mathematics and data analysis.

one needs even longer data spans, faster sampling, higher precision, more accurate timing and, in addition, nothing is independent. Practically, one can also say goodbye to concepts of mixing, stationarity, proper data, and similar concepts that one uses to prove theorems. ■

Acknowledgment

The authors would like to thank Prof. G. Pavlis and Dr. C. A. L. Haley for their careful and constructive reviews, Prof. C. Constable for needed LaTeX advice, C. Boteler for proofreading a draft manuscript, Prof. P. Jones for the European temperature data, and D. Gough for his numerous comments. They would also like to thank M.-L. Thomson for coordinating the

cross-continental response to reviewers, and D. Riebert for his outstanding sleuthing capabilities in finding the necessary files in D. J. Thomson’s filing system so that F. L. Vernon could respond to the reviewers. The results presented in this paper also rely on data collected at magnetic observatories, particularly those at Eskdalemuir, operated by the British Geological Survey; and Boulder, operated by the U.S. Geological Survey; and INTERMAGNET for promoting high standards of magnetic observatory practice (www.intermagnet.org). The Bartol Research Institute (BRI) of the University of Delaware, in collaboration with the Laboratory for Extraterrestrial Physics (LEP) at the Goddard Space Flight Center (GSFC), built and delivered a magnetometer instrument for the ACE mission. The Ulysses data came from ESA and NASA.

REFERENCES

- [1] A. Schuster, “On the investigation of hidden periodicities with application to supposed 26 day period of meteorological phenomena,” *Terrestrial Magn.*, vol. 3, pp. 13–41, 1898.
- [2] E. Parzen, “On asymptotically efficient consistent estimates of the spectral density function of a stationary time series,” *J. Roy. Stat. Soc.*, vol. B-20, pp. 303–322, 1958.
- [3] D. R. Brillinger, “Asymptotic properties of spectral estimates of second order,” *Biometrika*, vol. 56, pp. 375–390, 1969.
- [4] R. H. Farrell, “Asymptotic lower bounds for the risk of estimators of the value of a spectral density function,” *Z. Wahrscheinlichkeitstheorie verw. Gebiete*, vol. 49, pp. 221–234, 1979.
- [5] D. J. Thomson, “Spectrum estimation techniques for characterization and development of WT4 waveguide, Part I,” *Bell Syst. Tech. J.*, vol. 56, pp. 1769–1815, 1977.
- [6] D. J. Thomson, “Spectrum estimation techniques for characterization and development of WT4 waveguide, Part II,” *Bell Syst. Tech. J.*, vol. 56, pp. 1983–2005, 1977.
- [7] W. D. Warters, Ed., “WT4 millimeter waveguide system,” *Bell Syst. Tech. J.*, vol. 56, pp. 1825–1827, 1977.
- [8] D. J. Thomson, S. Harris, and P. E. Fox, “Mechanical gauging techniques for millimeter waveguide,” *Bell Syst. Tech. J.*, vol. 56, pp. 2007–2023, 1977.
- [9] D. J. Thomson, J. C. Anderson, J. W. Carlin, and T. J. West, “WT4 field evaluation test—Transmission medium achievements,” *Bell Syst. Tech. J.*, vol. 56, pp. 2157–2178, 1977.
- [10] G. G. Stokes, “On a method of detecting inequalities of unknown periods in a series of observations,” *Proc. R. Soc. Lond.*, vol. 29, pp. 122–123, 1879. G. G. Stokes, “Comment on the preliminary report to the committee on solar physics,” in *Mathematical and Physical Papers*, V. Cambridge, U.K.: Cambridge Univ. Press, 1905, pp. 52–53.
- [11] N. Wiener, “Generalized harmonic analysis,” *Acta Mathematica*, vol. 55, no. 1, pp. 117–258, 1930.
- [12] K. Hasselmann, W. H. Munk, and G. MacDonald, “Bispectra of ocean waves,” in *Time Series Analysis*, M. Rosenblatt, Ed. New York, NY, USA: Wiley, 1963, pp. 125–139.
- [13] H. He and D. J. Thomson, “The canonical bicoherence: Part I—Definitions, properties, and multitaper estimates,” *IEEE Trans. Signal Process.*, vol. 57, pp. 1273–1284, 2009.
- [14] I. Chuine et al., “Historical phenology: Grape ripening as a past climate indicator,” *Nature*, vol. 432, no. 7015, pp. 289–290, 2004.
- [15] J. Berger, P. Davis, and G. Ekström, “Ambient Earth noise: A survey of the global seismographic network,” *J. Geophys. Res.*, vol. 109, 2004, doi: 10.1029/2004JB003408.
- [16] D. J. Thomson and F. L. Vernon, “Unexpected, high-Q, low-frequency peaks in seismic spectra,” *Geophys. J. Int.*, vol. 202, pp. 1690–1710, 2015.
- [17] A. D. Chave, “Magnetotelluric data, stable distributions and impropriety: An existential combination,” *Geophys. J. Int.*, vol. 198, pp. 622–636, 2014.
- [18] D. J. Thomson, C. G. MacLennan, and L. J. Lanzerotti, “Propagation of solar oscillations through the interplanetary medium,” *Nature*, vol. 376, pp. 139–144, 1995.
- [19] D. J. Thomson, L. J. Lanzerotti, and C. G. MacLennan, “The interplanetary magnetic field: Statistical properties and discrete modes,” *J. Geophys. Res.*, vol. 106, pp. 15941–15962, 2001.
- [20] S. Ghosh, D. J. Thomson, W. H. Matthaeus, and L. J. Lanzerotti, “Coexistence of turbulence and discrete modes in the solar wind,” *J. Geophys. Res.*, vol. 114, no. A8, 2009.
- [21] D. J. Thomson, “Background magnetospheric variability as inferred from long time-series of GOES data,” *Dynamics of the earth’s radiation belts and inner magnetosphere*, *Geophys. Monogr. Ser.*, vol. 199, in D. Summers, I. R. Mann, D. N. Baker, and M. Schulz, Eds. Washington, DC, USA, pp. 225–241, 2012.
- [22] K. Nawa et al., “Incessant excitation of the Earth’s free oscillations,” *Earth Planets Space*, vol. 50, pp. 3–8, 1998.
- [23] N. Suda, K. Nawa, and Y. Fukao, “Earth’s background free oscillations,” *Science*, vol. 279, pp. 2089–2091, 1998.
- [24] T. Tanimoto, J. Um, K. Nishida, and N. Kobayashi, “Earth’s continuous oscillations observed on seismically quiet days,” *Geophys. Res. Lett.*, vol. 25, pp. 1553–1556, 1998.
- [25] W. Thomson (Lord Kelvin), “On the rigidity of the Earth,” *Philos. Trans. Roy. Soc. Lond.*, vol. 153, pp. 573–582, 1863.
- [26] W. Thomson (Lord Kelvin), “Dynamical problems regarding elastic spheroidal shells and spheroids of incompressible liquid,” *Philos. Trans. Roy. Soc. Lond.*, vol. 153, pp. 583–616, 1863.
- [27] F. A. Dahlen and J. Tromp, *Theoretical Global Seismology*. Princeton, NJ, USA: Princeton Univ. Press, 1998.
- [28] T. G. Masters and R. Widmer, “Free oscillations: Frequencies and attenuations,” in *Global Earth Physics*, T. J. Ahrens, Ed. Washington, DC, USA: AGU, 1995, pp. 104–125.
- [29] A. Deuss, J. Ritsema, and H. van Heijst, “A new catalogue of normal-mode splitting function measurements up to 10 mhz,” *Geophys. J. Int.*, vol. 193, pp. 920–937, 2013.
- [30] F. L. Vernon and D. J. Thomson, “Unexpected mode observations in the low frequency seismic spectrum,” *EOS Trans. AGU Jt. Assem. Suppl.*, vol. 88, 2007, Art. no. Abstract S34A-03.
- [31] D. J. Thomson and F. L. Vernon, “Characteristics and source of unexpected modes observed in the low frequency seismic spectrum,” in *Proc. AGU Fall Meet.*, 2007, Art. no. Abstract, Session S34A-04.
- [32] D. J. Thomson and F. L. Vernon, “Supplement to ‘unexpected, high-Q, low-frequency peaks in seismic spectra,’” *Geophys. J. Int.*, vol. 202, p. 14, 2015.
- [33] J. W. Harvey, “Helioseismology,” *Physics Today*, vol. 48, pp. 32–38, Oct. 1995.
- [34] D. J. Thomson, L. J. Lanzerotti, F. L. Vernon, III, M. R. Lessard, and L. T. P. Smith, “Solar modal structure of the engineering environment,” *Proc. IEEE*, vol. 95, pp. 1085–1132, 2007.
- [35] C. A. L. Haley, *Nonparametric and parametric methods for solar oscillation spectra*, Ph.D. dissertation, Dept. Math. Stat., Queen’s Univ., Kingston, ON, Canada, 2014.
- [36] D. J. Thomson and C. L. Haley, “Spacing and shape of random peaks in non-parametric spectrum estimates,” *Proc. Roy. Soc. A*, vol. 470, 2014, Art. no. 20140101.

- [37] A. Moghtaderi, D. J. Thomson, and G. Takahara, "Unfolding of aliased line component frequencies in bivariate time series," *Can. J. Stat.*, vol. 38, pp. 116–135, 2010.
- [38] D. J. Thomson, L. J. Lanzerotti, and C. G. MacLennan, "Low frequency (~ 2.19 day period) mode in records of interplanetary and central England temperature data," in *Proc. SOHO 6/GONG 98 Workshop, 'Struct. Dyn. Sun Sun-like Stars'*, 1998, vol. SP-418, pp. 967–971.
- [39] D. J. Thomson, "Some problems in the analysis of possibly cyclostationary data," in *Proc. IEEE 45th Asilomar Conf. Signals Syst. Comput.*, 2011, pp. 2040–2044.
- [40] J. Christensen-Dalsgaard, F. W. W. Dilke, and D. O. Gough, "The stability of a solar model to non-radial oscillations," *Monthly Notices Roy. Astron. Soc.*, vol. 169, pp. 429–445, 1974.
- [41] T. Appourchaux et al., "The quest for the solar g modes," *Astron. Astrophys. Rev.*, vol. 18, pp. 197–277, 2010.
- [42] M. F. Woodard and R. W. Noyes, "Change in solar oscillation eigenfrequencies with the solar cycle," *Nature*, vol. 318, pp. 449–450, 1985.
- [43] R. Howe, R. Komm, and F. Hill, "Solar cycle changes in GONG p-mode frequencies 1995–1998," *Astrophys. J.*, vol. 524, pp. 1084–1095, 1999.
- [44] R. Komm, R. Howe, and F. Hill, "Solar-cycle changes in GONG p-mode widths and amplitudes 1995–1998," *Astrophys. J.*, vol. 531, pp. 1094–1108, 2000.
- [45] W. J. Chaplin et al., "Source of excitation of low- l solar p modes: Characteristics and solar-cycle variations," *Monthly Notices Roy. Astron. Soc.*, vol. 314, pp. 75–86, 2000.
- [46] W. J. Chaplin et al., "Changes to low- l solar p-mode frequencies over the solar cycle: Correlations on different time-scales," *Monthly Notices Roy. Astron. Soc.*, vol. 322, pp. 22–30, 2001.
- [47] T. Toutain and A. G. Kosovichev, "Study of the solar cycle dependence of low-degree p-modes with Michaelson Doppler Imager and VIRGO," *Astrophys. J.*, vol. 622, pp. 1314–1319, 2005.
- [48] K. Jain, S. C. Tripathy, and F. Hill, "Solar activity phases and intermediate-degree mode frequencies," *Astrophys. J.*, vol. 695, pp. 1567–1576, 2009.
- [49] A. Jiménez, R. A. García, and P. L. Pallé, "The acoustic cutoff frequency of the sun and the solar magnetic activity cycle," *Astrophys. J.*, vol. 743, no. 2, p. 99, 2011.
- [50] J. Provost, G. Berthomieu, and P. Morel, "Low-frequency p- and g-mode solar oscillations," *Astron. Astrophys.*, vol. 353, pp. 775–785, 2000.
- [51] J. Beran, *Statistics for Long-Memory Processes*. New York, NY, USA: Chapman & Hall, 1994.
- [52] D. J. Thomson, "A test for 'long-memory' processes," in *Proc. IEEE Workshop Stat. Signal Process.*, St. Louis, MO, USA, 2003, pp. 541–544.
- [53] B. Kleiner, R. D. Martin, and D. J. Thomson, "Robust estimation of power spectra (with discussion)," *J. Roy. Stat. Soc. B*, vol. 41, pp. 313–351, 1979.
- [54] D. J. Thomson, "Spectrum estimation and harmonic analysis," *Proc. IEEE*, vol. 70, pp. 1055–1096, 1982.
- [55] L. Rayleigh, "On the spectrum of an irregular disturbance," *Philos. Mag.*, vol. 41, pp. 238–243, 1903.
- [56] F. J. Harris, "On the use of windows for harmonic analysis with the discrete Fourier transform," *Proc. IEEE*, vol. 66, pp. 51–83, 1978.
- [57] R. B. Blackman and J. W. Tukey, *The Measurement of Power Spectra*. New York, NY, USA: Dover, 1959.
- [58] R. P. Bogert, M. J. Healy, and J. W. Tukey, "The quefrency analysis of time series for echoes: Cepstrum, pseudo-autocovariance, cross-cepstrum and saphe cracking," in *Spectral Analysis of Time Series*, B. Harris, Ed. New York, NY, USA: Wiley, 1967, pp. 209–243.
- [59] M. A. Lombardi and G. K. Nelson, "WWVB: A half century of delivering accurate frequency and time by radio," *J. Res. Nat. Inst. Standards Technol.*, vol. 119, pp. 25–54, 2014.
- [60] M. A. Lombardi, "Time measurement," in *Measurement, Instrumentation, and Sensors Handbook*, 2nd ed., J. G. Webster and H. Eren, Eds. Boca Raton, FL, USA: CRC Press, 2014, pp. 41-1–41-21, ISBN: 9781439848838.
- [61] D. G. Childers, D. P. Skinner, and R. C. Kemerait, "The cepstrum: A guide to processing," *Proc. IEEE*, vol. 65, pp. 1428–1443, 1977.
- [62] D. J. Thomson, "Time series analysis of Holocene climate data," *Philos. Trans. Roy. Soc. Lond. A*, vol. 330, pp. 601–616, 1990.
- [63] H. Crámér, "On the theory of stationary random processes," *Ann. Math.*, vol. 41, pp. 215–230, 1940.
- [64] J. L. Doob, *Stochastic Processes*. New York, NY, USA: Wiley, 1953.
- [65] M. B. Priestley, *Spectral Analysis and Time Series*. San Diego, CA, USA: Academic, 1981.
- [66] A. Khintchine, "Korrelationstheorie der stationären stochastischen Prozesse," *Mathematische Annalen*, vol. 109, no. 1, pp. 604–615, 1934.
- [67] A. Einstein, "Méthode pour la détermination de valeurs statistiques d'observations concernant des grandeurs soumises à des fluctuations irrégulières," *Archives des Sciences*, vol. 37, pp. 254–256, 1914.
- [68] A. M. Yaglom, "Einstein's 1914 paper on the theory of irregularly fluctuating series of observations," *IEEE Signal Process. Mag.*, vol. 4, no. 4, pp. 7–11, 1987.
- [69] M. Loève, *Probability Theory*. Princeton, NJ, USA: Van Nostrand, 1963.
- [70] A. N. Kolmogorov, "On the $\Phi^{(n)}$ classes of Fortet and Blanc-Lapierre," *Theory Probab. Appl.*, vol. 5, p. 337, 1960.
- [71] D. Slepian and H. O. Pollak, "Prolate spheroidal wave functions, Fourier analysis and uncertainty—I," *Bell Syst. Tech. J.*, vol. 40, pp. 43–64, 1961.
- [72] D. Slepian, "Prolate spheroidal wave functions, Fourier analysis, and uncertainty V: The discrete case," *Bell Syst. Tech. J.*, vol. 57, pp. 1371–1429, 1978.
- [73] D. J. Thomson, "Quadratic-inverse spectrum estimates: applications to paleoclimatology," *Philos. Trans. Roy. Soc. Lond. A*, vol. 332, pp. 539–597, 1990.
- [74] E. J. Hannan, *Multiple Time Series*. New York, NY, USA: Wiley, 1970.
- [75] M. Taniguchi and Y. Kakizawa, *Asymptotic Theory of Statistical Inference for Time Series*. New York, NY, USA: Springer-Verlag, 2000.
- [76] H. O. Hartley, "The maximum F-ratio as a short-cut test for heterogeneity of variance," *Biometrika*, vol. 37, pp. 308–312, 1950.
- [77] P. Stoica and T. Sundin, "On nonparametric spectral estimation," *Circuits Syst. Signal Process.*, vol. 18, pp. 169–181, 1999.
- [78] M. M. Sondhi, "Random processes with specified spectral density and first-order probability density," *Bell Syst. Tech. J.*, vol. 62, pp. 679–701, 1983.
- [79] W. M. Gentleman, "An error analysis of Goertzel's (Watt's) method for computing Fourier coefficients," *Comput. J.*, vol. 12, pp. 160–164, 1969.
- [80] W. H. Munk and K. Hasselmann, "Super-resolution of tides," in *Hikada Volume*, K. Yoshida, Ed. Seattle, WA, USA: Univ. Washington Press, 1964, pp. 339–344.
- [81] K. S. Miller, *Complex Stochastic Processes*. Reading, MA, USA: Addison Wesley, 1974.
- [82] H. Scheffé, *The Analysis of Variance*. New York, NY, USA: Wiley, 1959.
- [83] R. A. Fisher, *Statistical Methods and Scientific Inference*, 3rd ed. New York, NY, USA: Macmillan, 1973.
- [84] W. S. Cleveland and S. J. Devlin, "Calendar effects in monthly time series: Detection by spectrum analysis and graphical methods," *J. Amer. Stat. Soc.*, vol. 75, pp. 487–496, 1980.
- [85] K. J. Rahim, *Applications of Multitaper Spectral Analysis to Nonstationary Data*, Ph.D. dissertation, Dept. Math. Stat., Queen's Univ., Kingston, ON, Canada, 2014.
- [86] W. Gleissberg, "The eighty-year sunspot cycle," *J. Brit. Astron. Assoc.*, vol. 68, pp. 148–152, 1958.
- [87] A. N. Peristykh and P. E. Damon, "Persistence of the Gleissberg 88-year solar cycle over the last 12,000 years: Evidence from cosmogenic isotopes," *J. Geophys. Res.*, vol. 108, p. A1, 2003.
- [88] J. L. Klein, *Statistical Visions in Time. A History of Time Series Analysis 1662–1938*. Cambridge, U.K.: Cambridge Univ. Press, 1997.
- [89] D. J. Thomson, "The seasons, global temperature, and precession," *Science*, vol. 268, pp. 59–68, 1995.
- [90] C. L. Wolff, "Linear r-modes below the Sun's convective envelope," *Astrophys. J.*, vol. 531, pp. 591–598, 2000.
- [91] N. S. Dzhililov and J. Staude, "Eigenoscillations of the differentially rotating Sun II. Generalization of the Laplace tidal equation," *Astron. Astrophys.*, vol. 421, pp. 305–322, 2004.
- [92] W. J. Chaplin, *The Music of the Sun: The Story of Helioseismology*. Oxford, U.K.: Oneworld, 2006.
- [93] H. Hotelling, "Relations between two sets of variates," *Biometrika*, vol. 28, pp. 321–377, 1936.
- [94] N. Giri, "On complex analogues of T^2 and R^2 tests," *Ann. Math. Stat.*, vol. 36, pp. 664–670, 1965.
- [95] G. E. P. Box, "Non-normality and tests on variances," *Biometrika*, vol. 40, pp. 318–335, 1953.
- [96] R. D. Martin and D. J. Thomson, "Robust-resistant spectrum estimation," *Proc. IEEE*, vol. 70, pp. 1097–1115, 1982.

- [97] A. D. Chave, D. J. Thomson, and M. E. Ander, “On the robust estimation of power spectra, coherences, and transfer functions,” *J. Geophys. Res.*, vol. 92, pp. 633–648, 1987.
- [98] M. E. Kappus and F. L. Vernon, “Acoustic signature of thunder from seismic records,” *J. Geophys. Res.*, vol. 96, pp. 10989–11006, 1991.
- [99] R. Mellors, F. L. Vernon, and D. J. Thomson, “Detection of dispersive signals using multitaper dual-frequency coherence,” *Geophys. J. Int.*, vol. 135, pp. 146–154, 1998.
- [100] K. Q. Lepage and D. J. Thomson, “Spectral analysis of cyclostationary time-series: A robust method,” *Geophys. J. Int.*, vol. 179, pp. 1199–1212, 2009.
- [101] A. D. Chave and D. J. Thomson, “A bounded influence regression estimator based on the statistics of the hat matrix,” *J. Roy. Stat. Soc. C, Appl. Stat.*, vol. 52, pp. 307–322, 2003.
- [102] A. D. Chave and D. J. Thomson, “Bounded influence magnetotelluric response function estimation,” *Geophys. J. Int.*, vol. 157, pp. 988–1006, 2004.
- [103] N. L. Johnson, S. Kotz, and N. Balakrishnan, *Continuous Univariate Distributions*, 2nd ed. New York, NY, USA: Wiley, 1995.
- [104] J. Christensen-Dalsgaard, “Helioseismology,” *Rev. Modern Phys.*, vol. 74, pp. 1073–1129, 2002.
- [105] M. Stix, *The Sun: An Introduction*, 2nd ed. Berlin, Germany: Springer-Verlag, 2004.
- [106] P. M. Shearer, *Introduction to Seismology*. Cambridge, U.K.: Cambridge Univ. Press, 1999.
- [107] M. L. Goldstein, D. A. Roberts, and W. H. Matthaeus, “Magnetohydrodynamic turbulence in the solar wind,” *Annu. Rev. Astron. Astrophys.*, vol. 33, pp. 283–326, 1995.
- [108] R. T. Wicks, T. S. Horbury, C. H. K. Chen, and A. A. Schekochihin, “Power and spectral index anisotropy of the entire inertial range of turbulence in the fast solar wind,” *Monthly Notices Roy. Astron. Soc., Lett.*, vol. 407, no. 1, pp. L31–L35, 2010.
- [109] B. Bavassano, D. Dobrowolny, F. Mariani, and N. F. Ness, “Radial evolution of power spectra of interplanetary Alfvénic turbulence,” *J. Geophys. Res.*, vol. 87, pp. 3617–3622, 1982.
- [110] T. S. Horbury, M. Forman, and S. Oughton, “Anisotropic scaling of magnetohydrodynamic turbulence,” *Phys. Rev. Lett.*, vol. 101, no. 17, 2008, Art. no. 175005.
- [111] E. S. Pearson and H. O. Hartley, *Biometrika Tables for Statisticians*. Cambridge, U.K.: Cambridge Univ. Press, 1970.
- [112] P. Delache and P. H. Scherrer, “Detection of solar gravity mode oscillations,” *Nature*, vol. 306, pp. 651–653, 1983.
- [113] P. L. Pallé, “The search for solar gravity modes,” *Adv. Space Res.*, vol. 11, no. 4, pp. 29–38, 1991.
- [114] P. Kumar, E. J. Quataert, and J. N. Bahcall, “Observational searches for solar g-modes: Some theoretical considerations,” *Astrophys. J.*, vol. 458, pp. L83–L85, 1996.
- [115] J. T. Nolte and E. C. Roelof, “Large-scale structure of the interplanetary medium I: High coronal source longitude of the quiet-time solar wind,” *Solar Phys.*, vol. 33, pp. 241–257, 1973.
- [116] J. T. Nolte and E. C. Roelof, “Large-scale structure of the interplanetary medium II: Evolving magnetic configurations deduced from multi-spacecraft observations,” *Solar Phys.*, vol. 33, pp. 483–504, 1973.
- [117] J. Schou, A. G. Kosovichev, P. R. Goode, and W. A. Dziembowski, “Determination of the Sun’s seismic radius from the SOHO Michelson Doppler Imager,” *Astrophys. J.*, vol. 489, pp. L197–L200, 1997.
- [118] L. J. Lanzerotti, D. J. Thomson, and C. G. MacLennan, “Engineering issues in space weather,” in *Modern Radio Science*, M. A. Stuchly, Ed. Oxford, U.K.: Oxford Univ. Press, 1999, pp. 25–50.
- [119] D. H. Boteler, R. J. Pirjola, and H. Nevanlinna, “The effects of geomagnetic disturbances on electrical systems at the Earth’s surface,” *Adv. Space Res.*, vol. 22, pp. 17–27, 1998.
- [120] W. H. Barlow, “On the spontaneous electrical currents observed in the wires of the electric telegraph,” *Philos. Trans. Roy. Soc. Lond.*, vol. 139, pp. 61–72, 1849.
- [121] A. D. Chave and A. G. Jones, Eds., *The Magnetotelluric Method*. Cambridge, U.K.: Cambridge Univ. Press, 2012.
- [122] L. J. Lanzerotti, D. J. Thomson, A. Meloni, L. V. Medford, and C. G. MacLennan, “Electromagnetic study of the Atlantic continental margin using a section of a transatlantic cable,” *J. Geophys. Res.*, vol. 91, pp. 7417–7427, 1986.
- [123] S. Haykin, D. J. Thomson, and J. Reed, “Spectrum sensing for cognitive radio,” *Proc. IEEE*, vol. 97, pp. 849–877, 2009.
- [124] G. B. Airy, “First analysis of one hundred and seventy-seven magnetic storms, registered by the magnetic instruments in the Royal Observatory, Greenwich, from 1841 to 1857,” *Philos. Trans. Roy. Soc. Lond.*, vol. 153, pp. 617–648, 1863.
- [125] D. J. Thomson, L. J. Lanzerotti, and C. G. MacLennan, “Coherent frequency variations in electron fluxes at 1 and 5 AU in the inner heliosphere,” in *Proc. ACE2000 Symp. Acceleration Transp. Energetic Particles Observed Heliosphere* vol. 528, pp. 278–281, 2000.
- [126] S. C. Webb, “The Earth’s hum: The excitation of Earth normal modes by ocean waves,” *Geophys. J. Int.*, vol. 174, pp. 542–566, 2008.
- [127] T. Forbriger, “Reducing magnetic field induced noise in broad-band seismic recordings,” *Geophys. J. Int.*, vol. 169, pp. 240–258, 2007.
- [128] R. A. García et al., “Low-degree low-order solar p modes as seen by GOLF on board SOHO,” *Solar Phys.*, vol. 200, pp. 361–379, May 2001.
- [129] D. Salabert, J. Leibacker, T. Appourchaux, and F. Hill, “Measurement of low signal-to-noise ratio solar p-modes in spatially resolved helioseismic data,” *Astrophys. J.*, vol. 696, pp. 653–667, 2009.
- [130] A.-M. Broomhall et al., “Definitive Sun-as-a-star p-mode frequencies: 23 years of BiSON observations,” *Monthly Notices Roy. Astron. Soc.*, vol. 396, pp. L100–L104, 2009.
- [131] S. M. Kay and S. L. Marple, “Spectrum analysis—A modern perspective,” *Proc. IEEE*, vol. 69, pp. 1380–1419, 1981.
- [132] R. D. Martin and R. H. Zamar, “Asymptotically Min-Max bias robust M-Estimates of scale for positive random variables,” *J. Amer. Stat. Soc.*, vol. 84, pp. 494–501, 1989.
- [133] D. Camuffo and P. D. Jones, Eds., *Improved Understanding of Past Climatic Variability From Early Daily European Instrumental Sources*. Dordrecht, The Netherlands: Kluwer, 2002.
- [134] H. Bergström and A. Moberg, “Daily air temperature and pressure series for Uppsala (1722–1998),” *Climatic Change*, vol. 53, pp. 213–252, 2002.
- [135] T. R. Karl et al., “Testing for bias in the climate record,” *Science*, vol. 271, pp. 1879–1883, 1996.
- [136] D. J. Thomson, “Dependence of global temperatures on atmospheric CO₂ and solar irradiance,” *Proc. Nat. Acad. Sci. USA*, vol. 94, pp. 8370–8377, 1997.
- [137] P. J. Rousseeuw, “Least median of squares regression,” *J. Amer. Stat. Assoc.*, vol. 79, pp. 871–880, 1984.
- [138] H. L. Hurd and A. Miamee, *Periodically Correlated Random Sequences*. New York, NY, USA: Wiley, 2007.
- [139] A. Napolitano, *Generalizations of Cyclostationary Signal Processing*. Chichester, West Sussex, U.K.: IEEE Press/Wiley, 2012.
- [140] E. Rieger et al., “A 154-day periodicity in the occurrence of hard solar flares?,” *Nature*, vol. 312, pp. 623–625, 1984.
- [141] D. J. Thomson, “Jackknifing multitaper spectrum estimates,” *IEEE Signal Process. Mag.*, vol. 24, no. 7, pp. 20–30, Jul. 2007.
- [142] A. Moberg, H. Bergström, J. R. Krigsman, and O. Svanerud, “Daily air temperature and pressure series for Stockholm (1756–1998),” *Climatic Change*, vol. 53, pp. 171–212, 2002.
- [143] D. Camuffo, “History of the long series of daily air temperature in Padova (1725–1998),” *Climatic Change*, vol. 53, pp. 7–75, 2002.
- [144] L. J. Lanzerotti et al., “Heliosphere instrument for spectra, composition, and anisotropy at low energies,” *Astron. Astrophys. Suppl. Ser.*, vol. 92, pp. 349–363, 1992.
- [145] B. Stewart and W. Dodgson, “Preliminary report to the committee on solar physics on the evidence in favour of the existence of certain short periods common to solar and terrestrial phenomena,” *Proc. Roy. Soc. Lond.*, vol. XXIX, pp. 303–324, 1879.
- [146] D. R. Brillinger, *The Collected Works of John W. Tukey: Volume I Time Series: 1949–1964*. Belmont, CA, USA: Wadsworth, 1984.
- [147] D. R. Brillinger, *The Collected Works of John W. Tukey: Volume II Time Series: 1965–1984*. Belmont, CA, USA: Wadsworth, 1984.

ABOUT THE AUTHORS

David J. Thomson (Life Fellow, IEEE) was born in Saint John, NB, Canada. He received the B.Sc. degree in mathematics and physics from Acadia University, Wolfville, NS, Canada, in 1965 and the M.S. and Ph.D. degrees in electrical engineering from Polytechnic Institute of Brooklyn, Brooklyn, NY, USA, in 1967 and 1971, respectively.



From 1965 to 1977, he was a Member of Technical Staff with Bell Telephone Laboratories, Inc., Murray Hill, NJ, USA. From 1977 to 1984, he was a Distinguished Member of Technical Staff with Bell Telephone Laboratories, Inc. He was responsible for quality control on the WT4 Millimeter Waveguide System and for both the circuit design and software for a microprocessor-controlled modem for Rayleigh fading channels in the first cellular phone system. From 1984 to 2001, he was a Research Scientist with Bell Telephone Laboratories, Inc. In 1985, he was H. Burr Steinback Visiting Scholar at Woods Hole Oceanographic Institution, Woods Hole, MA, USA. From 1990 to 1996, he was a consultant for the Neurological Institute at Columbia University, New York, NY, USA. In 1993, he was a visiting Professor in Statistics at Princeton University, Princeton, NJ, USA. Since 2002, he has been a Professor in Mathematics and Statistics at Queen's University, Kingston, ON, Canada. He has taught courses at Princeton and Stanford, gave the Houghton lectures at Massachusetts Institute of Technology, and was a participant at the Isaac Newton Institute at the University of Cambridge. From 2002 through 2015, he held the Canada Research Chair in Statistics and Signal Processing in the Department of Mathematics and Statistics of Queen's University. He has been a coinvestigator on the HISCALE instrument of the *Ulysses* spacecraft since 1993 and was awarded a Killam fellowship for the analysis of this data. He is a holder of over 25 patents. In addition to time series analysis and spectrum estimation, his current research interests are analysis of global climate data, space physics, and seismology.

Dr. Thomson is a member of the American Geophysical Union and the American Statistical Association, and a Professional Statistician in the Statistical Society of Canada. He is a Chartered Statistician and a

Fellow of the Royal Statistical Society and a Professional Engineer. He was a member of the Panel on Sensors and Electron Devices of the Army Research Laboratory Technical Assessment Board, Chairman of Commission C of USNC-URSI and an Associate Editor for *Radio Science*. He was an Associate Editor for Communications Theory and for Detection and Estimation of the IEEE TRANSACTIONS ON INFORMATION THEORY. In 2010, he was elected a Fellow of the Royal Society of Canada.

Frank L. Vernon, III was born in Pasadena, CA, USA. He received the B.A. degree in physics with a specialization in Earth sciences and the Ph.D. degree in Earth sciences from the University of California, San Diego, La Jolla, CA, USA, in 1977 and 1989, respectively.



Starting in 1977, he has worked at the Cecil and Ida Green Institute of Geophysics and Planetary Physics, Scripps Institution of Oceanography, University of California, San Diego, as a Developmental Technician, Staff Research Associate (1980), Postdoctoral Researcher (1989), and Research Scientist (1990). Since 2004, he has been the Director of the Array Network Facility. He is the principal investigator (PI) on the ANZA broadband and strong motion seismic network that has operated since 1982 providing real-time seismic monitoring capability for southernmost California. He is a co-PI on very dense seismic deployment around the San Jacinto fault zone, focusing on earthquake source physics, fault structure, and providing real-time seismic monitoring capability for southernmost California. In addition, he is a PI on the HPWREN program creating a large-scale wireless high-performance data network that is being used for interdisciplinary research and education applications, as well as a research test bed for wireless technology systems in general.

Dr. Vernon is a life member of the American Geophysical Union, a member of the American Meteorological Society, and a member of the Seismological Society of America. He is an editor for the AGU journal *Earth and Space Sciences*.